https://doi.org/10.5194/cp-2024-25
Preprint. Discussion started: 15 April 2024

Climate of the Past
Discussions

A sub-fossil coral Sr/Ca record documents meridional variability of the Intertropical Convergence Zone in the eastern Indian Ocean

Miriam Pfeiffer[1], Hideko Takayanagi[2], Lars Reuning[1], Takaaki K. Watanabe[1,3], Saori Ito[1,3], Dieter Garbe-Schönberg[1], Tsuyoshi Watanabe[3,4,5], Chung-Che Wu[6], Chuan-Chou Shen[7,8], Jens Zinke[9], Geert-Jan A. Brummer[10], Sri Yudawati Cahyarini[11]

[1]Institute of Geosciences, Kiel University, Kiel, 24118, Germany
[2]Institute of Geology and Paleontology, Graduate School of Science, Tohoku University, Aramaki-Aza-Aoba 6-3, Sendai 980-8578, Japan
[3]KIKAI Institute for Coral Reef Sciences, Kikai Town, Kagoshima 891-6151, Japan.
[4]Department of Natural History Sciences, Faculty of Science, Hokkaido University, Sapporo, 060-0810, Japan
[5]Research Institute for Humanity and Nature (RIHN), Kyoto 603-8047, Japan
[6]College of Marine Sciences and Engineering, Nanjing Normal University, Nanjing, 210023, China
[7]High-Precision Mass Spectrometry and Environment Change Laboratory (HISPEC), Department of Geosciences, National Taiwan University, Taipei, 10617, Taiwan ROC
[8]Research Center for Future Earth, National Taiwan University, Taipei, 10617, Taiwan ROC
[9]School of Geography, Geology and the Environment, University of Leicester, Leicester, LE1 7RH, UK
[10]Department of Ocean Systems, Royal Netherlands Institute for Sea Research (NIOZ), and Utrecht University, 1790 AB Den Burg, The Netherlands
[11]Res. Group of Paleoclimate & Paleoenvironment, Res. Centr. for Climate and Atmosphere, National Research and Innovations Agency (BRIN), Republic of Indonesia

Correspondence to: Miriam Pfeiffer (Miriam.pfeiffer@ifg.uni-kiel.de)

Abstract. Sea surface temperature (SST) variability in the south-eastern tropical Indian Ocean is crucial for rainfall variability in Indian Ocean rim countries. A large body of literature has focused on zonal variability associated with the Indian Ocean Dipole (IOD), but it is unclear whether meridional shifts in the position of the Intertropical Convergence Zone (ITCZ), which at present co-vary with the IOD, may also occur independently. We have developed a new, monthly resolved Sr/Ca record from a sub-fossil coral cored at Enggano Island (Indonesia, 5° S, 102° E). Core sections containing diagenetic phases are omitted from the SST reconstruction. U/Th dating shows that the Sr/Ca-based SST record extends from 1917-1868 and from 1861-1823 with a relative age uncertainty of ±2.4 years (2σ). At Enggano Island, coastal upwelling and cooling in austral spring is coupled to the position of the ITCZ, and impacts SST seasonality. The sub-fossil coral indicates an increase in SST seasonality due to enhanced austral spring cooling between 1917 and 1855, which we attribute to stronger SE winds and a northward shift in the position of the ITCZ in austral spring. A nearby sediment core indicates SST cooling and a shallowing of the thermocline prior to ~1930. These results are consistent with an increase in the North-South SST gradient in the eastern Indian Ocean calculated from historical temperature data, that is not seen in the zonal SST gradient. We conclude that the relationship between meridional and zonal variability in the eastern Indian Ocean is non-stationary and influenced by long-term temperature trends.

https://doi.org/10.5194/cp-2024-25
Preprint. Discussion started: 15 April 2024

1 Introduction

Sea surface temperature (SST) variability in the south-eastern (SE) tropical Indian Ocean is crucial for rainfall variability in Indian Ocean rim countries (Weller et al., 2014; Cai et al., 2013). A large body of literature has focused on the Indian Ocean Dipole (IOD) (Saji et al., 1999; Webster et al., 1999; Ummenhofer et al., 2009a; Ummenhofer et al., 2009b; Cai et al., 2013; Saji and Yamagata, 2003; Behera et al., 2005; Ashok et al., 2003), a zonal mode characterized a reversal of the east-west SST gradient in the tropical Indian Ocean, causing droughts in Indonesia and Australia, and enhanced rainfall and flooding in equatorial East Africa (Ummenhofer et al., 2009a; Ummenhofer et al., 2009b; Saji et al., 1999; Behera et al., 2005; Ashok et al., 2003). Comparatively little attention has been paid to meridional (north-south) SST gradients and related circulation anomalies over the SE tropical Indian Ocean, although these can also induce significant droughts in Indonesia, and flooding in southern India and Sri Lanka, via northward shifts of the Intertropical Convergence Zone (ITCZ) in austral spring (Fig. 1) (Weller et al., 2014; Weller and Cai, 2014).

The eastern Indian Ocean north of 10°S features the most intense atmospheric convection in the Indian Ocean basin (Fig. 1) (Schott et al., 2009). Meridional displacements of the ITCZ are driven by ocean-atmosphere interactions in the SE tropical Indian Ocean, which include monsoon-induced coastal upwelling in austral spring (September-November) and active SST-thermocline feedbacks (Susanto et al., 2001; Webster et al., 1999; Cai et al., 2013; Saji and Yamagata, 2003; Weller et al., 2014). Coastal upwelling is driven by strong, southeasterly (SE) winds along the coasts of Java and Sumatra associated with the South Asian Summer Monsoon (Susanto et al., 2001) (Fig. 2, Fig. A1). Anomalously strong SE winds enhance coastal upwelling and cooling, which may shift the position ITCZ to the equator, and may trigger a reversal of the zonal SST gradient in the tropical Indian Ocean (that is, a positive IOD event) (Saji et al., 1999; Fischer et al., 2005). In the satellite era, positive IOD events and northward displacement of the ITCZ are tightly coupled (Weller et al., 2014; Weller and Cai, 2014) and northward shifts of the ITCZ may be seen as a characteristic of positive IOD events (Fig. 1). However, future projections suggest that meridional shifts in the position of the ITCZ may uncouple from the IOD due to the rapidly warming Asian landmass in response to greenhouse warming and, as a result, faster warming rates in the north-eastern Indian Ocean relative to the south-east (Weller and Cai, 2014; Weller et al., 2014).

SST variability in the SE equatorial Indian Ocean is poorly represented in historical, gridded data of SSTs, which do not adequately capture the non-linear ocean-atmosphere feedbacks in the region (Yang et al., 2020; Pfeiffer et al., 2022; Cai et al., 2013). Therefore, observational studies on the relationship between meridional and zonal SST variability are limited to the last ~40 years in which we have satellite data of SST (Weller et al., 2014; Weller and Cai, 2014). Coral Sr/Ca ratios measured at monthly resolution were shown to provide a realistic representation of SST variability in the SE tropical Indian Ocean, as, unlike historical SSTs interpolated from sparse data, the coral proxy data is not compromised by non-linear ocean-atmosphere feedbacks (Yang et al., 2020; Pfeiffer et al., 2022; Cahyarini et al., 2021). To date, however, coral studies of historical variability in the SE tropical Indian Ocean have mainly focused on zonal variability associated with the IOD (Abram et al., 2015; Abram et al., 2008; Abram et al., 2007; Abram et al., 2020).

Here, we present a new, monthly-resolved Sr/Ca record from a sub-fossil *Porites* coral drilled at Enggano Island (Sumatra, Indonesia). Our new coral Sr/Ca record derives from a large massive colony found in a dead, partially bio-eroded reef (Fig. 3). U/Th dating indicates that the base of the coral record is 1823 ±2.4 (2σ) years old and the youngest sections extend to the early 20th century. Extensive screening with a state-of-the-art Hitachi SU 3900 Scanning electron microscope (SEM) was performed to identify and omit intervals with minor early marine diagenesis and to ensure the reliability of the Sr/Ca data. Combining our new coral data with previously published coral Sr/Ca records from Enggano Island that extend from 2008-1930 (Pfeiffer et al., 2022), we investigate the relationship between meridional and zonal SST variability in the SE Indian Ocean prior to the satellite era.

https://doi.org/10.5194/cp-2024-25
Preprint. Discussion started: 15 April 2024

Climate of the Past
Discussions

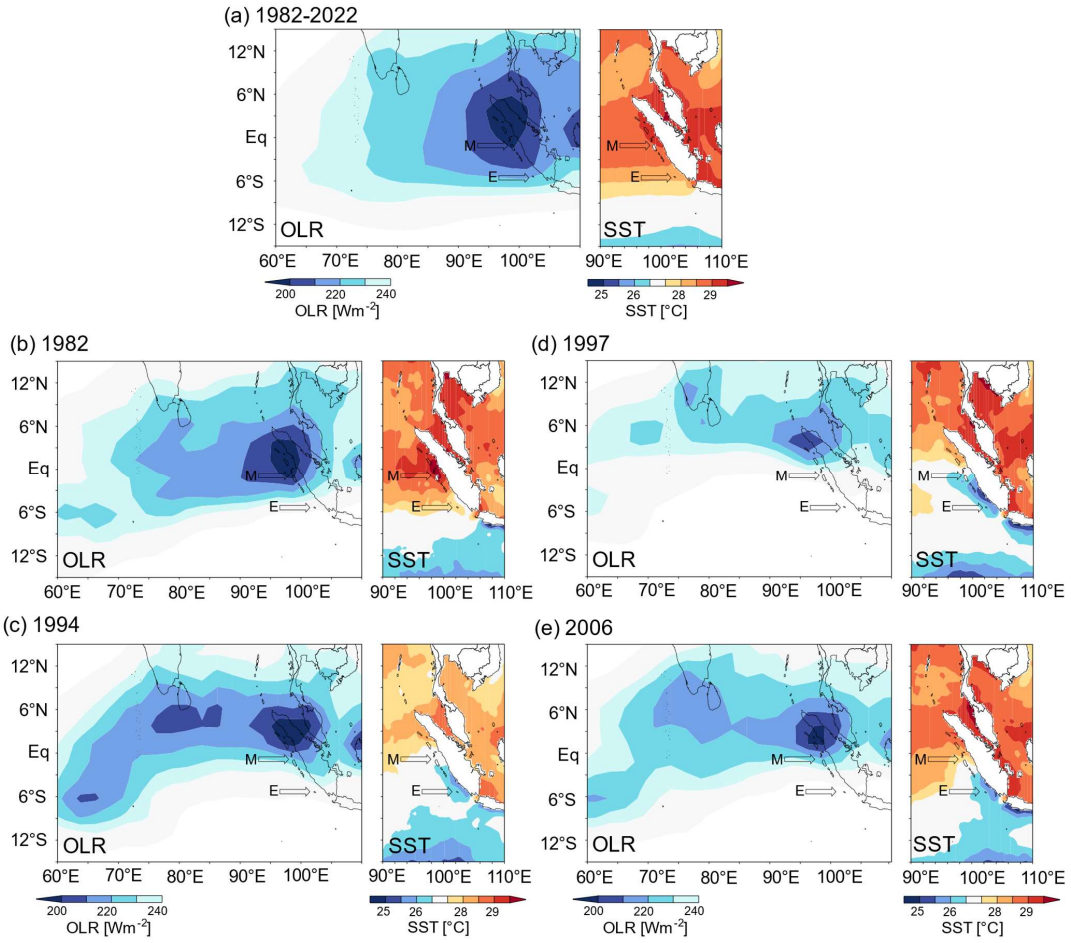

Figure 1: Austral spring outgoing longwave radiation (OLR) and SST in the eastern Indian Ocean. (a) Mean September-November OLR (left) (Schreck et al., 2018) and AVHRR OI SST (right) (Huang et al., 2021) from 1982-2022. (b) September-November OLR (left) and SST (right) for the moderate positive IOD event of 1982. (c) Same as (b) but for the extreme positive IOD event of 1994 (d) Same as (b) for the extreme positive IOD event of 1997, (e) same as (b) for the extreme positive IOD event of 2006. OLR ≤ 240 W m^{-2} countour indicates the position of the ITCZ. Note the correspondence of the 27.5 °C and 28 °C countours at the coast of Sumatra and the latitude of the ITCZ. Arrows mark location of Enggano (E) and Mentawai (M). Charts computed at the knmi climate explorer (https://climexp.knmi.nl).

https://doi.org/10.5194/cp-2024-25
Preprint. Discussion started: 15 April 2024

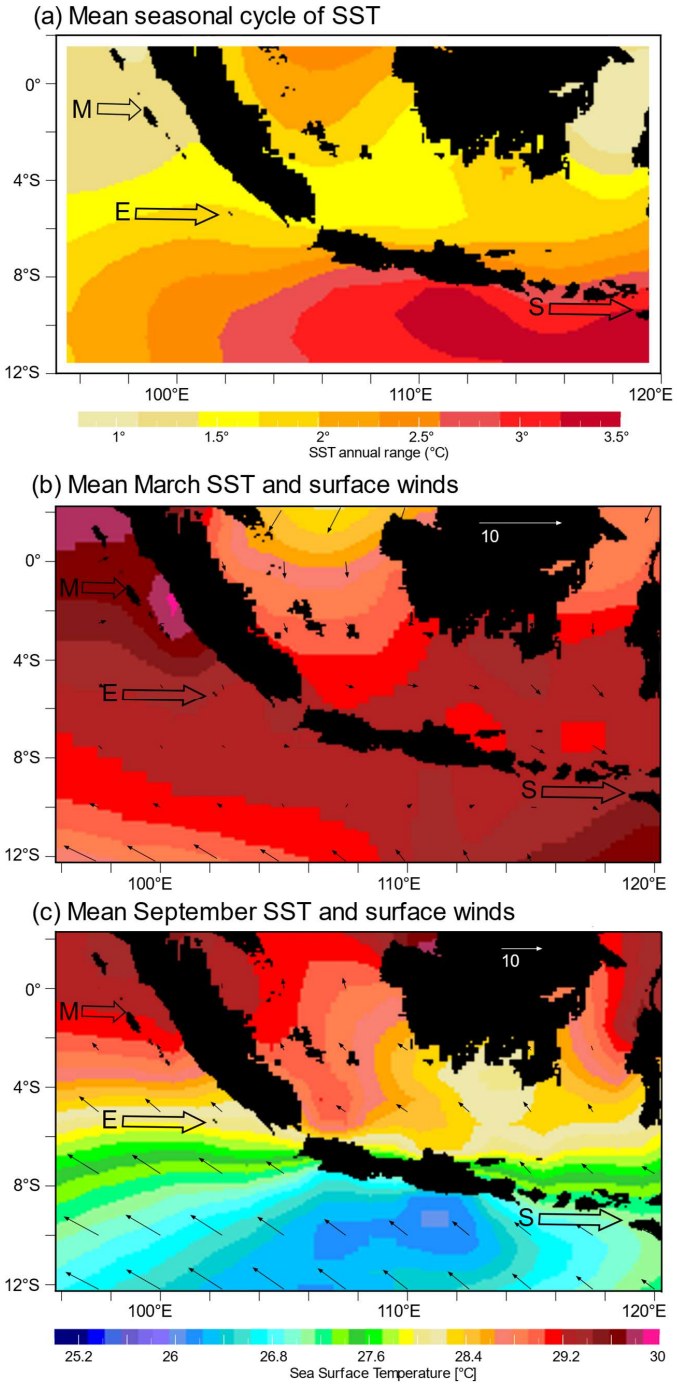

Figure 2: SST seasonality and surface winds in the SE Indian Ocean. (a) The amplitude of the mean seasonal cycle of SST (in °C) decreases from >3 °C to 1 °C from Java to Sumatra. (b) In austral fall, mean SSTs (colors) are warm and uniform, and surface winds (vectors) are weak. (c) In austral spring, strong, alongshore SE winds (vectors) lead to cooling off the coast to Java and Sumatra, and large meridional differences in mean SSTs (colors). Open arrows in (a) and (b) mark location of Enggano (E), northern Mentawai (M), and Sumba Island (S). Note the steep SST gradients south of Enggano. SST data from OI SST (Reynolds et al., 2002), wind data from (Kalnay et al., 1996). Charts computed at https://iridl.ldeo.columbia.edu/.

https://doi.org/10.5194/cp-2024-25
Preprint. Discussion started: 15 April 2024

2 Study area

Enggano Island lies ~200 km off the coast of south-eastern Sumatra at 5 °S, 102 °E (Fig. 3). It is the southernmost island on the fore-arc ridge offshore Sumatra, which also comprises the Mentawai Island chain located further north (3-1 °S, 98-100 °E). In austral spring, SE winds associated with the South Asian summer monsoon generate coastal upwelling and cooling off Java and Sumatra (Fig. 2) (Susanto et al., 2001). The standard deviation of monthly mean SST reveals the centers of upwelling (Fig. 3, Fig. A1). Upwelling first develops off the coast of Java in June, and then propagates north-westwards (Fig. A1). It reaches Enggano in July, and extends to the Mentawai Islands in October (Fig. A1). In November-December, westerly winds terminate coastal upwelling and SE Indian Ocean SSTs are generally warm with comparatively little spatial variability in austral fall (Fig. 2).

The strength of the SE winds in austral spring thus primarily determines the seasonal cycle of SSTs in the SE Indian Ocean, causing steep gradients of seasonality, from > 3 °C off Java to ~1.5-1.0 °C off Sumatra, which reflect spatial variations in the frequency of occurence of coastal upwelling and cooling in August-October (Fig. 2, Fig. 3). At Enggano, austral spring SSTs are colder than at the northern Mentawai Islands, SST seasonality is larger, and annual mean SSTs are lower (Fig. 2, Fig. 3). Furthermore, Enggano is situated in a region where meridional gradients in the magnitude of August-October cooling are particularly steep, which translates into steep meridional gradients in SST seasonality near Enggano Island (Fig. 2).

Off the coast of Java, the SE winds cause strong upwelling and cooling every year (Susanto et al., 2001), mean August-October SSTs are low (<27 °C) (Fig. 2, Fig. 3). The distribution of mean August-September SSTs is symmetric (Fig. 3). On interannual time scales, stronger-than-normal SE winds lead to an anomalous strengthening of coastal upwelling and cooling off Sumatra that may lead to (I) a northward shift of the ITCZ, which then lies north of Enggano Island (Fig. 1) (Weller et al., 2014), and (II) a reversal of the zonal SST gradient in the tropical Indian Ocean and the development of a positive IOD event (Saji et al., 1999; Yang et al., 2020; Ng et al., 2015). Extreme positive IOD events coupled with a strong northward shift of the ITCZ lead to a cooling of SSTs down to 25 °C that extends to the equator (Fig. 1, Fig. A2). The occasional occurrence of extreme positive IOD events in an equatorial region featuring warm surface waters in normal years is reflected in a strong negative skewness of August-October SSTs off Sumatra (Fig. 3) (Yang et al., 2020) and an enhanced seasonal cycle in these years. In contrast, anomalous austral spring cooling during moderate positive IOD events is weaker and spatially restricted to the south-eastern coast of Sumatra, where Enggano is located, and the Java and Timor Sea (Fig. 1, Fig. A2). In addition to IOD-related SST variability (Pfeiffer et al., 2022), the corals from Enggano Island should therefore be sensitive recorders of changes in the strength of the SE winds and the position of the ITCZ (Fig. 1, Fig. 2).

https://doi.org/10.5194/cp-2024-25
Preprint. Discussion started: 15 April 2024

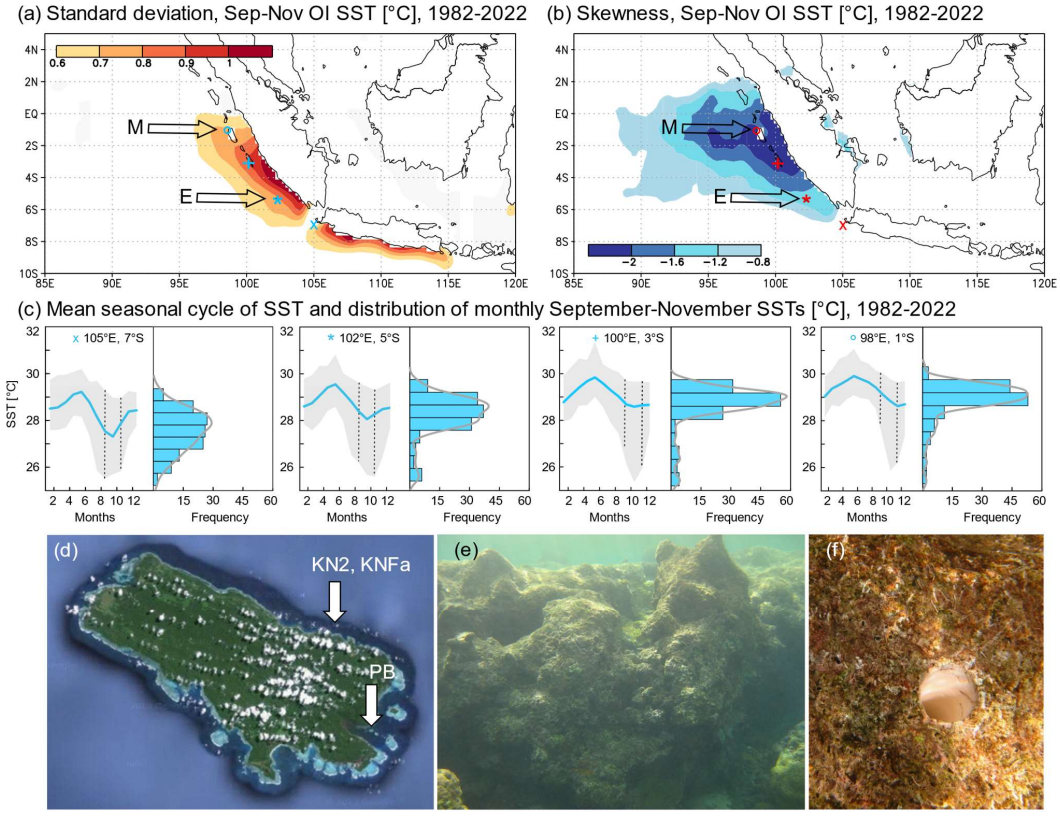

Figure 3: Location and climatic setting of Enggano Island. (a) The standard deviation of September-November SST indicates areas of coastal upwelling off the coast of Java and Sumatra. (b) The skewness of September-November SSTs reflects interannual coastal upwelling events. Arrows in (a) and (b) mark location of Enggano Island (E) and northern Mentawai Island (M). Charts were computed at the knmi climate explorer (https://climexp.knmi.nl). (c) Mean seasonal cycles of satellite SST (thick blue lines) from northern Java to central Sumatra with 99 % confidence levels (grey shading). SST grids are selected with a latitudinal spacing of 2°, symbols indicate their position in (a) and (b). Histograms show the distribution of monthly mean SSTs in the August-October season. At all sites, SST minima are ~25 °C, but progressively higher mean August-October SSTs occur at sites North of 7°S, where only extreme positive IOD events cause intense coastal upwelling. This results in a negative skewness in the 99% confidence levels around the August-October SSTs (indicated by dashed black lines), in the histograms of August-October SSTs, and in (b). Histograms computed using PAST (Hammer et al., 2001). SST data is from AVHRR OI SST (1/4° grids) (Huang et al., 2021). (d) Satellite image of Enggano Island showing fringing reefs from GoogleEarth. At its longest section, Enggano Island is 35 km long. Modern cores were drilled at the southeastern (PB) and northeastern (KN2) coast. A subfossil coral (KNFa) was drilled next to core KN2. (e) Dead reef on the northeastern coast of Enggano Island and (f) bio-eroded surface of sub-fossil coral colony with open borehole. Photos from S.Y. Cahyarini.

3 Methods and data

3.1 Coral collection

In an August 2008 field campaign, sub-fossil, dead fringing reefs were discovered around Enggano Island (Sumatra, Indonesia) in a water depth of ~3m (Fig. 3). A large massive *Porites* coral was found and a 1.83 m coral core (KNFa) was drilled using a pneumatic drill powered by Scuba tanks. After drilling, the core KNFa was cut into 5 mm thick slabs and prepared for subsampling following standard procedures (Cahyarini et al., 2014b). X-rays (Fig. 4) and luminescence scans (Fig. A3) were made at the Royal Netherlands Institute for Sea Research (NIOZ) on untreated coral slabs to reveal the coral's seasonal banding pattern and to indicate potential zones of diagenesis. The KNFa core shows multiple density bands per year that do not allow a precise chronology based on annual bands, but a good correlation of corresponding sections on adjacent coral slabs (Fig. 4, Fig. A3).

https://doi.org/10.5194/cp-2024-25
Preprint. Discussion started: 15 April 2024

Two modern *Porites* corals (KN2 and PB) were collected from living corals during the same field campaign, and their Sr/Ca records were published previously (Pfeiffer et al., 2022). The two modern corals extend from 2008-1930, and are used here for comparison with the sub-fossil coral data.

3.2 Diagenetic screening

Based on X-ray images and luminescence scans (Fig. 4, Fig. A3), potential diagenetic alteration was assessed, using representative samples for mineralogical and microscopic analysis. Conventional, destructive analysis included powder X-ray diffraction (XRD, n=3), thin-section (n=3) and scanning electron microscopy (SEM, n= 5) on gold-coated coral blocks (see Fig. 4 for sample location).

Furthermore, we conducted higher resolution, non-destructive mineralogical and microscopic analysis directly on the coral slabs, parallel to the proxy sampling tracks. The 2-D-XRD system Bruker D8 ADVANCE GADDS was used for non-destructive XRD point-measurements with a calcite detection limit of ~ 0.2 % (Smodej et al., 2015). The nineteen 2-D-XRD measurements resulted in a sampling resolution of one spot analysis every ~ 7 cm. Sections showing a mottled appearance on the luminescence scans were selected for non-destructive SEM analysis with the Hitachi SU3900 system. The extra-large chamber of this SEM system can accommodate coral slabs up to 30 cm in length (Fig. A4, A5). The analyses were carried out in low vacuum mode (30 and 50Pa) using an ultra-variable-pressure detector (UVD) and a backscattered electron detector (BSE). This low vacuum mode allows the coral slabs to be analyzed continuously and directly along the proxy sample track without the need for coating with conductive materials such as gold.

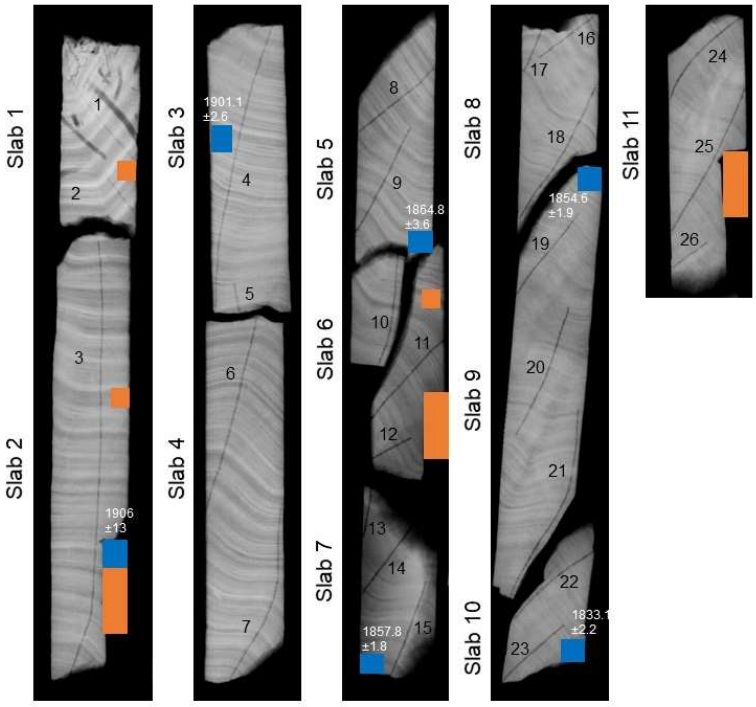

Figure 4: X-ray image of the sub-fossil coral core KNFa from Enggano Island. Core slabs and sampling transects for Sr/Ca analysis are numbered (data see Fig. 5). Blue squares indicate samples taken for U/Th dating and their ages. Note: the core shows prominent sub-annual bands that allow a good match between different slabs. Some sections of the core were cut off to assess preservation using conventional, destructive methods (powder XRD, thin section and SEM analysis using gold-coated stubs of coral). Small orange boxes indicate locations for SEM samples. Large orange boxes indicate locations for combined powder-XRD, SEM and thin-section samples. See text for discussion.

https://doi.org/10.5194/cp-2024-25
Preprint. Discussion started: 15 April 2024

3.3 Sr/Ca analysis

The KNFa core was subsampled for Sr/Ca analysis at 1 mm intervals, i.e. at approximately monthly resolution. For each subsample, we extracted 0.1-0.2 mg of coral powder for Sr/Ca analysis using a hand-held drill. Sr/Ca ratios were measured at Kiel University using a Spectro Ciros CCD SOP inductively coupled plasma optical emission spectrometer (ICP-OES). Elemental emission signals were simultaneously collected and subsequently processed following a combination of techniques described by Schrag (1999) and Villiers et al. (2002). Average analytical precision of Sr/Ca measurements as estimated from sample replicates was typically around 0.08 % RSD or less than 0.1 °C. All coral Sr/Ca ratios were normalized to an in-house standard calibrated against JCp-1 (8.838 mmol mol^{-1}) (Hathorne et al., 2013). Measurements of JCp-1 had a median of 8.832 mmol mol^{-1}, and a standard deviation of 0.009 (1σ) or 0.10 % RSD.

The chronology of the coral Sr/Ca records is developed using anchor points following the approach of Cahyarini et al. (2021): we assigned September to the Sr/Ca maxima (on average the coldest month). The data is then linearly interpolated to 12 monthly values per year.

3.4 U/Th Dating and chronology

The age of KNFa was estimated by U/Th dating at National Taiwan University, following the methods of (Shen et al., 2012). After chemical separation for U and Th isotopes in a clean room, the samples were analysed with a multi-collector inductively coupled plasma mass spectrometer (MC-ICP-MS, NEPTUNE). Results are shown in Table A1.

A floating chronology was estimated following the approach of Domínguez-Villar et al. (2012). The age of the coral record was estimated from the intercept of the linear regression between the U/Th ages and the annual cycles of Sr/Ca (Fig. 5), assuming that the slope of this regression is one, using Eq. 1:

$$No.of\ annual\ cycles = U - Th\ age + b\ , \qquad (1)$$

where "b" is the floating age. With this regression, the differences between U/Th ages and corresponding Sr/Ca ages are minimal (0.1 years for the overall time series). The age uncertainty of the floating chronology was estimated with a Monte Carlo approach (20,000 loops) using the 2σ U/Th error. The base of the KNFa Sr/Ca record is dated to 1823 ± 2.4 (2σ) years CE.

Combining the U/Th ages with the coral density banding and growth rates suggest that the coral died in the early 1930s, although the exact timing cannot be determined due to extensive bioerosion at the top of the coral. It is unclear what caused the death of the sub-fossil coral (and the fringing reef where the core was taken), but possible candidates include several major earthquakes centered on Enggano island in the 1930s with magnitudes ≥ 7 (Newcomb and McCann, 1987), or severe cold anomalies, possibly coupled with red tides, due to extreme IOD-induced upwelling events (Abram et al., 2003).

3.5 Coral Sr/Ca-SST conversion

To avoid biases from so-called 'vital effects' that affect mean coral Sr/Ca ratios (e.g. Cahyarini et al., 2011; Ross et al., 2019), all coral Sr/Ca records were centered to their mean and converted to SST units assuming a coral Sr/Ca-SST relationship of -0.06 mmol mol^{-1} per 1 °C (Corrège, 2006; Ross et al., 2019; Watanabe and Pfeiffer, 2022), hereafter referred to as SST_{center}. This slope is consistent with the coral Sr/Ca-SST calibrations of the two modern corals KN2 and PB from Enggano Island with satellite SST data (Pfeiffer et al., 2022), which is available since 1982. SST_{center} inferred from KN2 and PB Sr/Ca data shows the same distribution as satellite SSTs in the grid including Enggano Island (Pfeiffer et al., 2022) (Fig. A7).

https://doi.org/10.5194/cp-2024-25
Preprint. Discussion started: 15 April 2024

4. Results

4.1 Coral preservation

The three conventional powder and nineteen 2D-XRD-analysis (see Fig. 4 for location) indicate that the subfossil core KNFa is purely aragonitic and does not contain any calcitic phases. The analysis of the conventional SEM samples and thin-sections (see Fig. 4 for location) indicates a generally excellent preservation with pristine, smooth skeletal surfaces, except for the SEM sample near the top of the coral core, which shows minor (< 5 µm-long) but pervasive aragonite cementation. To evaluate the extent of potential diagenetic alteration we scanned the entire length of the Sr/Ca sampling tracks on slabs 1 and 2, using the uncoated coral slabs (see Methods and Fig. A4, A5). This analysis confirmed that minor fibrous aragonite cements (5 to 10 µm long) and incipient dissolution are restricted to the upper ~ 14 cm of the coral core, which also shows abundant bioerosion traces (Fig. 4: Slab 1), and a dull to mottled appearance in luminescence scans (Fig. A3). We therefore subsequently used the SEM to scan all core intervals that show similar dull colors in luminescence scans. After the proxy measurements, we additionally checked all intervals containing prominent Sr/Ca anomalies for diagenetic changes based on SEM observations directly on the coral slabs. Using this method, we were able to identify patches of aragonite needle cements (5 to 10 µm long) (Fig. A5), that had escaped detection with our previous standard screening protocol. Sr/Ca data from all intervals showing patchily distributed aragonite cements (sampling transects 1, 2, top of 3, base of 9 to top of 15, see Fig. 4 and 5) were excluded from further interpretation, since even light levels of aragonite cementation may lead to higher bulk Sr/Ca-values and consequently a cold bias in temperature reconstructions (Enmar et al., 2000; Allison et al., 2007; Hendy et al., 2007; Sayani et al., 2011).

4.2 The sub-fossil coral Sr/Ca record

Figure 5 shows the coral Sr/Ca data as measured along the maximum growth axis of core KNFa, prior to interpolation to monthly values and prior to omitting intervals affected by diagenesis. Therefore, each dot represents one Sr/Ca measurement of a discrete subsample. Also indicated are the slabs of the coral core and the sampling transects of Sr/Ca analysis (in color, numbers of slabs and transects are also shown on the x-ray images, see Fig. 4). Data from overlapping transects are shown on top of each other. The first Sr/Ca measurement on each new slab is marked as 'slab boundary'; note that this data overlaps with data from the previous slab due to the coral's growth. After measuring the Sr/Ca ratios along the entire core at 1 mm intervals, we subsequently omit data from transects were early marine diagenesis was detected by non-destructive SEM analysis from further processing (see 'coral preservation'). These sections are masked out in grey in Figure 5.

In the intervals not affected by diagenesis, the Sr/Ca record of KNFa shows clear seasonal cycles which can be counted visually to develop an age model. By combining this internal coral chronology with the U/Th ages (see methods), we estimate that the KNFa Sr/Ca record extends from 1917-1868 and 1861-1823 (Fig. S5, Fig. S7, Fig. 6), i.e. it encompasses a total of 94 years with 87 years of record, with a relative age uncertainty of ±2.4 years (2σ). The Sr/Ca data from well-preserved sections of the core show an excellent reproducibility between sampling transects (note that slight offsets along the X-axis reflect differences in coral growth), i.e. the means and variations of measured Sr/Ca ratios are consistent throughout the core (Fig. 5).

The distribution of the measured Sr/Ca data of KNFa is investigated in intervals representing approximately equal amounts of data points. The Sr/Ca distribution is symmetric with a standard deviation of 0.05 to 0.053 mmol mol^{-1} in the upper sections of the coral core (slab 3 to top of slab 8), symmetric with a standard deviation of 0.035 mmol mol^{-1} from slab 8 to 9, and positively skewed with a standard deviation of 0.044 mmol mol^{-1} from slab 10 to 11. Note, however, that the positive skewness of Sr/Ca data from slab 10 and 11 is due to only four consecutive Sr/Ca data of up to 9.148 mmol mol^{-1} on slab 11 (which cannot be attributed to diagenesis). The reduction in standard deviation is due to a persistent change in the nature of the Sr/Ca record that occurs ~850 mm below the top of the coral (Fig. 5).

https://doi.org/10.5194/cp-2024-25
Preprint. Discussion started: 15 April 2024

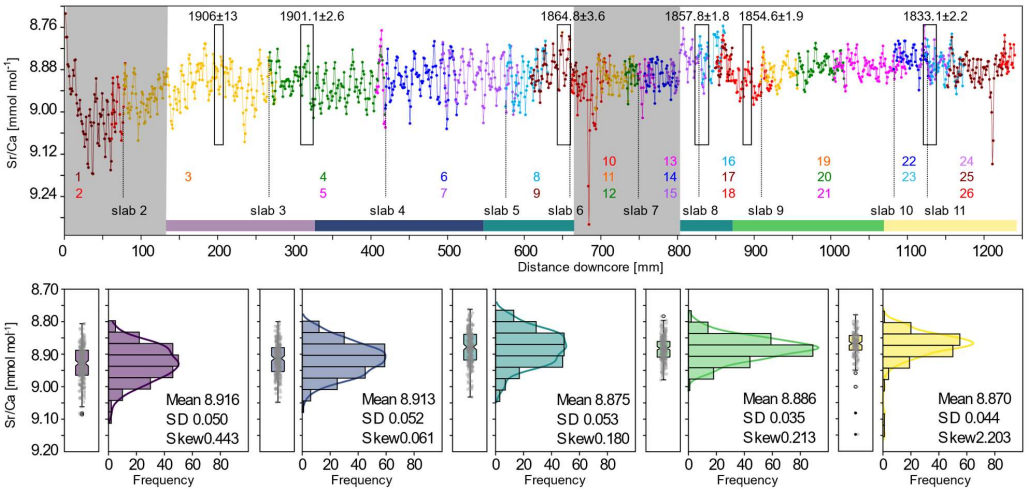

Figure 5: Sub-fossil coral Sr/Ca data of core KNFa. Top panel: Measured Sr/Ca data of core KNFa vs. distance downcore (in mm). Each dot corresponds to one Sr/Ca measurement. Sampling transects are highlighted by different colors and numbered (bottom) (see Fig. 4 for location of transect). Grey shading marks intervals discarded from further interpretation as diagenetic alterations have been detected. Sections sampled for U/Th ages are shown by black rectangles. Color bars at the bottom indicate data included in the histograms, box- and jitter-plots shown in the bottom panel. Note the reduction in the standard deviation of measured Sr/Ca data at a depth of ~860 mm. Histograms computed using PAST (Hammer et al., 2001).

5. Discussion

5.1 Sub-fossil coral Sr/Ca data and diagenesis

Sub-fossil corals are an important archive to extent the instrumental record back into pre-industrial periods (Abram et al., 2020; Cobb et al., 2013; Sanchez et al., 2020). Living corals may grow continuously for more than 300 years (Zinke et al., 2004; DeLong et al., 2013; Linsley et al., 2000), but in many key regions of climate variability, extreme climate disturbances can contribute to their demise (Abram et al., 2003). However, applying the coral Sr/Ca thermometer to sub-fossil corals is challenging as relatively minor amounts of diagenetic alteration can already significantly distort the Sr/Ca thermometer (Allisson et al. 2007; Sayani et al., 2011; Sayani et al., 2022). Standard screening protocols based on destructive analysis of discrete samples by thin-section, XRD and SEM are not always sufficient to map out the often patchily distributed diagenetic phases in corals. In this study, only the diagenetic alteration at the top of the core was identified using conventional methods, while other patches of aragonite cements in slabs 5 to 7 were not detected. A way to circumvent this problem are non-destructive methods that can be used to screen coral slabs for diagenetic phases at high spatial resolution (Murphy et al., 2017). 2D-XRD analysis non-destructively quantifies the amount of calcite cements directly on the coral slab with mm-scale spatial resolution (Smodej et al., 2015; Leupold et al., 2021). However, other types of diagenetic alteration such as aragonite dissolution or aragonite cements cannot be detected by XRD (Allison et al., 2007; McGregor and Abram, 2008). Typically, aragonite cements are patchily distributed (Nothdurft and Webb, 2009; (Sayani et al., 2011; Sayani et al., 2022; Smodej et al., 2015), while adjacent areas of the coral's skeleton are unaffected (Zinke et al., 2016). Such local concentrations of diagenetic phases could introduce spikes in the Sr/Ca data or other proxy records, that could be misinterpreted as climate events (Quinn and Taylor, 2006). Use of an SEM with an extra-large chamber in combination with an ultra-variable pressure detector (Fig. A4), allowed us to scan entire core slabs along the proxy sampling tracks without the need for a conductive coating. Our record showed an extreme spike with a Sr/Ca ratio of 9.32 mmol mol^{-1} on transect 10 of slab 6 (Fig. 5). We were able attribute this extreme Sr/Ca spike to a patch of aragonite cement and to omit this 'false alarm' spike from further interpretation. This is important as at Enggano Island, such a spike would indicate an extreme positive IOD event with a cooling exceeding -5 °C.

https://doi.org/10.5194/cp-2024-25
Preprint. Discussion started: 15 April 2024

Events of this magnitude do not occur in recent time periods captured in the satellite record, and including this Sr/Ca data would have significantly impacted the climatic interpretation of core KNFa. Furthermore, the interval from the base of transect 9 to the top of transect 15 lacks clear seasonal variability in coral Sr/Ca, which is normally indicative of irregularly distributed patches of diagenetic cements impacting the Sr/Ca proxy, but since Enggano Island lies in a region with low seasonality, confirmation by SEM is important to map the extend of this zone. We conclude that it is important to clearly identify and delimit zones of even minor, early marine diagenesis in young, sub-fossil corals, preferable directly adjacent to the sampling transect of Sr/Ca analysis, as a basis for a subsequent climatic interpretation of the Sr/Ca data from sub-fossil corals (Sayani et al., 2022).

5.2 SST_{center} inferred from Enggano coral Sr/Ca data since 1823

Two modern coral Sr/Ca records (KN2 and PB) from Enggano Island were shown to closely track satellite SSTs that extend back to 1982 and to reliably record IOD variability, while gridded SST products interpolated from sparse historical data systematically underestimated extreme positive IOD events, even in the time period covered by satellites (Yang et al., 2020; Pfeiffer et al., 2022). This has been attributed to non-linear ocean atmosphere feedbacks in the south-eastern equatorial Indian Ocean that are not captured in the statistical methods used to interpolate historical SSTs from sparse observational data (Ng et al., 2015; Yang et al., 2020).

In this study, we re-evaluate the two single-core modern coral Sr/Ca records as a basis for the interpretation of the sub-fossil KNFa Sr/Ca record. We limit the interpretation of KNFa on aspects clearly seen in each single modern coral record. A composite computed from both cores provides an improved quantitative SST reconstruction (Pfeiffer et al., 2022), but for the interpretation of KNFa, this would be misleading. Figure A8 compares the coral Sr/Ca records of the two modern corals from Enggano Island with the sub-fossil record of KNFa after interpolation to monthly resolution. The most notable feature of the two modern coral Sr/Ca records are large positive Sr/Ca anomalies during the extreme positive IOD events of 1997, 1994, 1967, 1963 and 1961 (Fig. A8, Fig. 6) (Pfeiffer et al., 2022).

Violin and box plots of the monthly Sr/Ca data from each Enggano coral record are computed in time intervals spanning approximately 20 years (note that some variations arise from the total length of the time periods covered by the coral records). The median Sr/Ca ratios of KN2 and PB are offset by ~0.065 by ±0.0156 mmol mol^{-1} (1σ) (Fig. A8), which would correspond to a difference >1 °C assuming a Sr/Ca-SST relationship of -0.06 mmol mol^{-1} $°C^{-1}$ (Corrège, 2006; Watanabe and Pfeiffer, 2022), if temperature related. However, offsets in mean or median coral Sr/Ca ratios from different coral colonies are due to so-called 'vital effects' (Villiers et al., 1994; Watanabe and Pfeiffer, 2022; Ross et al., 2019) and have been seen even in coral Sr/Ca records from adjacent colonies growing next to temperature loggers (Leupold et al., 2019). For climate reconstructions from corals, it is important that this offset remains constant within a coral core, which has been demonstrated in numerous calibration studies (e.g. Ross et al., 2019). The constant difference in median Sr/Ca ratios between KN2 and PB supports the use of Enggano coral Sr/Ca ratios as indicators of SST variability (Fig. A8). (Fig. A8).

Both modern coral cores show similar distributions of monthly Sr/Ca data in each ~20-year time interval, with a strong positive skewness in time periods with extreme positive IOD events (2008-1990; 1969-1950) and a symmetric distribution in periods without extreme positive IOD events (Fig. A8). This includes the number and spread of outliers (which reflect extreme positive IOD events). The KNFa record, in contrast, shows symmetric distributions, albeit with a larger spread around the median (indicating a larger standard deviation of the Sr/Ca data) in all time windows between 1917-1855. This is also seen in the raw, un-interpolated Sr/Ca data of KNFa (Fig. 5). Between 1854 and 1923, the spread of coral Sr/Ca around the median reduces again to ranges seen in the modern cores, with outliers arising from a few extreme positive Sr/Ca values in 1825 indicating an extreme positive IOD event. The reduction in the standard deviation prior to 1855 is also seen in the raw, un-interpolated Sr/Ca data of core KNFa (Fig. 5).

https://doi.org/10.5194/cp-2024-25
Preprint. Discussion started: 15 April 2024

Recent extreme positive IOD events (2006, 1997, 1994, 1967, 1963 and 1961) are recorded in the SST_{center} records inferred from KN2 and PB Sr/Ca data, which each indicate a cooling < -4 °C at Enggano Island (Fig. 6, Pfeiffer et al., 2022). These extreme events also impacted the meridional SST gradient in the eastern equatorial Indian Ocean, with warm anomalies in the north and cold anomalies in the south, and caused a northward contraction of the ITCZ (Fig. 1, Fig. A9). August-October mean SST_{center} data of KN2 and PB is highly correlated with the meridional SST gradient in the eastern Indian Ocean (Fig. A9).

The sub-fossil coral KNFa shows only one large Sr/Ca anomaly in 1825, near the end of the coral record, which is on par with these recent extreme events (Fig. 6). SEM images confirm that the 1825 event cannot be attributed to diagenetic changes and we therefore attribute it to an extreme positive IOD event – the only one in the interval from 1854 to 1823 recorded at Enggano Island. Between 1917-1855, KNFa shows several cold anomalies in the austral spring (Fig. 6, Fig. A8), the largest of which (1916, 1907, 1889, 1885, 1881) are comparable to 2006, a slightly weaker extreme positive IOD event in the modern record (Pfeiffer et al., 2022; Yang et al., 2020).

To better characterize the changes in SST variability inferred from coral Sr/Ca over time, we computed wavelet power spectra. In the two modern records, extreme positive IOD events are clearly seen as concentrations of power at seasonal to interannual periodicities (Fig. 6), and seasonal variability is much weaker than interannual variability. This changes in the sub-fossil record of KNFa between 1917-1855. In this period, seasonal variability is the dominant signal, while interannual variability is weaker than in the modern data (Fig. 6). Prior to 1855, seasonal variability reduces again, and the single extreme positive IOD event in 1825 is again seen as a concentration of power at seasonal to interannual periodicities (Fig. 6). These results suggest changes in the SST variability in the SE Indian Ocean that include changes in seasonality in addition to interannual variability associated with the IOD.

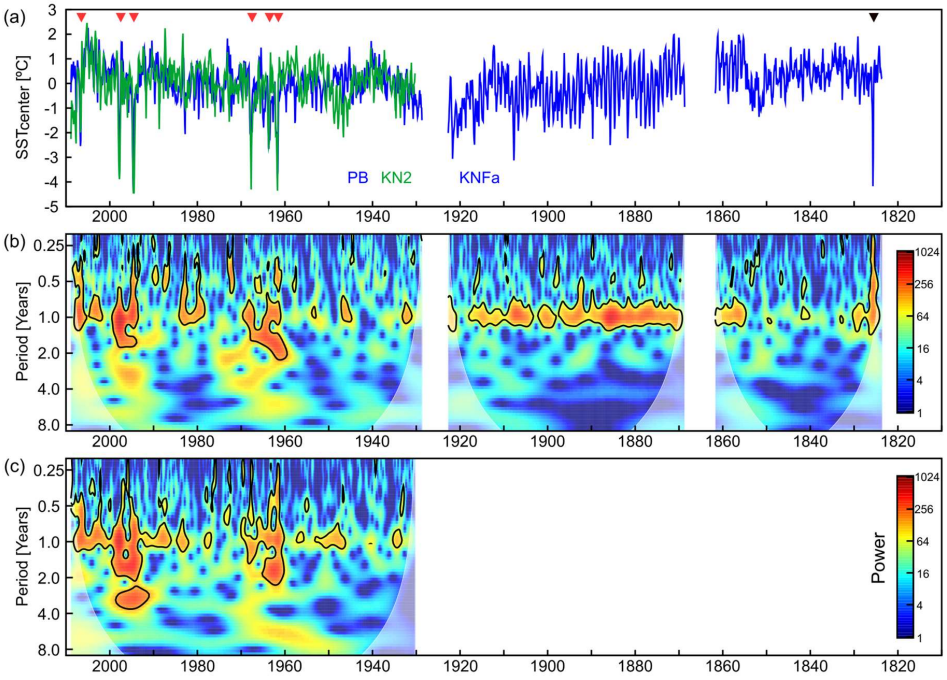

Figure 6: Modern and sub-fossil, monthly SST_{centre} inferred from Enggano coral Sr/Ca ratios. (a) The SST_{centre} record from Enggano comprises two modern (PB, KN2) and one sub-fossil core (KNFa) and extends from 2008-1930, 1917-1869 and 1861-1823. Thin blue and green lines are monthly data, thick red solid and dashed lines are 10-year running means. Note that the sub-fossil coral chronology is based on U/Th dating with an age uncertainty of ±2.4 years (2σ). Extreme positive IOD events lead to cooling of ≥ -4 °C in 2006,1997,1994, 1967, 1963 and 1961 (red arrows). The sub-fossil core KNFa shows an extreme positive IOD event on par with the event in the 1997 in ~1825 (black arrow). (b) Wavelet power spectra of SST_{centre} time series of core PB and KNFa. (c) same as (b) but for core KN2. Power spectra of PB and KN2 are dominated by extreme positive IOD events (red arrows in a). SST_{centre} of KNFa shows enhanced seasonal variability between 1917 and 1855. Prior to 1855, seasonal variability is comparable to PB and KN2, with one extreme positive IOD event in 1823. Wavelet Power spectra were computed in R using the Morlet Wavelet.

https://doi.org/10.5194/cp-2024-25
Preprint. Discussion started: 15 April 2024

5.3 SST seasonality between 1917 and 1855

Based on the evolution of SST seasonality at Enggano Island portrayed in the wavelet power spectra (Fig. 6), we computed mean seasonal cycles of SST_{centre} and their 99 % confidence intervals for the time periods from 2008-1930, 1917-1855 and 1854-1823 (Fig. 7). These time periods were chosen in order to compare periods with weak and strong SST seasonality. Modern SST_{centre} seasonality inferred from coral Sr/Ca varies from 1.1 °C (KN2) to 1 °C (PB) between 2008 and 1930, consistent with satellite data of SST that is available since 1982 (Fig. 7). SST_{centre} seasonality increases to ~1.9 °C between 1917-1855 and then decreases again to modern values (~1 °C) between 1854 and 1823. The difference in the mean seasonal cycles between 2008-1930 and 1917-1855 is statistically significant at the 99% confidence level, while the mean seasonal cycles between 2008-1930 and 1854-1823 are statistically indistinguishable (Fig. 7). In the two modern SST_{centre} records from Enggano Island, the extreme positive IOD events (2006, 1997, 1994, 1967, 1963 and 1961) cause a strong skewness (Fig. 8, Fig. A7, Fig. A8). This skewness is reflected in the 99 % confidence intervals around August-October mean SST_{centre} in Figure 7, that is also seen in present-day satellite SSTs centered at Enggano Island (Fig. 3).

In contrast, in the time period from 1917-1855, when SST_{center} seasonality is significantly enhanced, the distribution of August-October SST_{center} is symmetric (Fig. 7, Fig. 8). In this period, strong August-October cooling occurs in almost every year (Fig. 6), although there is also some interannual variability. The magnitude of the mean seasonal SST_{center} cycle as well as the distribution of August-October SST_{center} compare much better to satellite SSTs seen today at ~7°S, i.e. off northern Java (Fig. 8). Furthermore, maximum SSTs occur 1-2 months earlier than in modern coral SST_{centre} and satellite SSTs, suggesting an early onset of austral spring cooling. Our results suggest stronger SE winds extending further to the northwest along the Java-Sumatra coast, and an expansion of the region with strong wind- and upwelling-induced cooling in austral spring. We therefore believe that the increase in the seasonal cycle of SST_{center} between 1855-1917 reflects an earlier onset coupled with an increase in the strength of the SE winds in July-October, which then penetrated further north along the Java-Sumatra coast in almost every year, and led to stronger cooling at Enggano Island. This would imply a northward shift in the mean position of the ITCZ, a northward contraction of the eastern Indian Ocean Warm Pool and a stronger meridional SST gradient in the eastern Indian Ocean (Weller and Cai, 2014; Weller et al., 2014). We favor this interpretation over a change in zonal variability associated with the IOD, as the IOD is by definition an interannual phenomenon of climate variability. At present, positive IODs are relatively rare, impacting the 99 % confidence levels around the August-October mean SSTs, rather than the monthly mean values of August-October SSTs (i.e. the mean seasonal cycle itself). Seasonality in the eastern tropical Indian Ocean, including the onset of the SE winds of Java and Sumatra, is primarily driven by the Asian summer monsoon and the position of the ITCZ (Fig. 1, Fig. 2).

https://doi.org/10.5194/cp-2024-25
Preprint. Discussion started: 15 April 2024

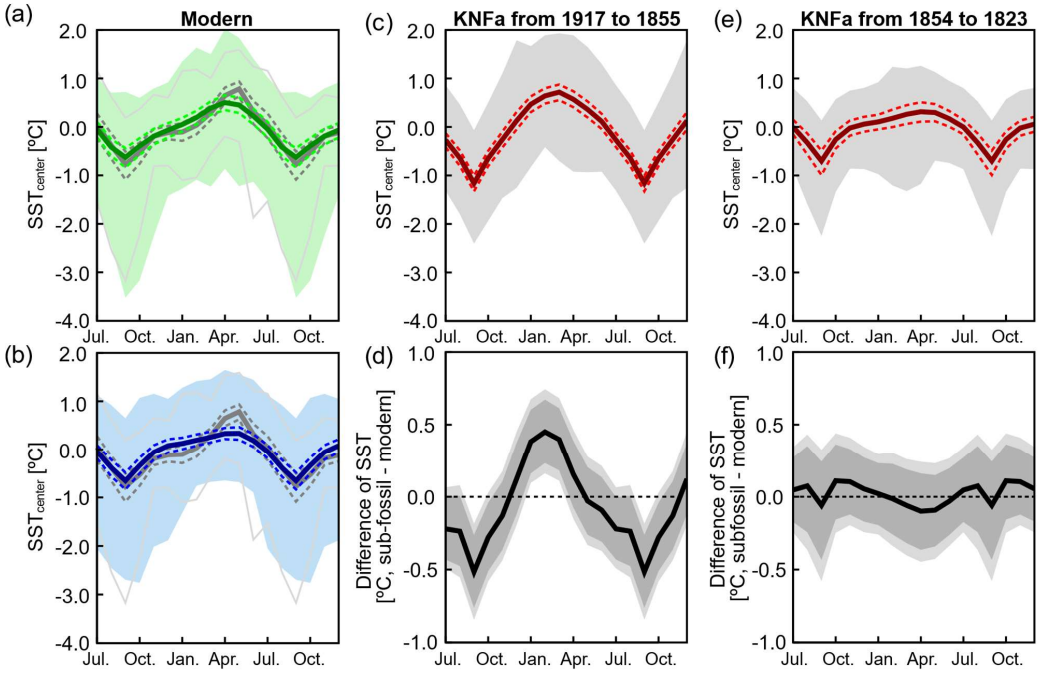

Figure 7: Mean seasonal cycles of SST$_{center}$ derived from modern and historical Enggano corals. (a) 2008-1930, core KN2 (in green; solid line is monthly mean, dashed green lines are ±1σ, shading indicates 99 % percentiles of monthly means). Satellite SST data (Huang et al., 2021) (mean removed, dark grey and dashed lines; thin grey lines are 99 % percentiles) are shown for comparison. (b) Same as (a), but for core PB (in blue; solid line is monthly mean, dashed green lines are ±1σ, shading indicates 99 % percentiles of monthly means). (c) Same as (a) but for core KNFa in the time period from 1917-1855 (in red; solid line is monthly mean, dashed green lines are ±1σ, grey shading indicates 99 % percentiles of monthly means), (d) Difference of mean seasonal cycles: (2008-1930) minus (1917-1855), with 95 and 99 % confidence levels (dark and light shading, respectively) based on a 20 000 sample Monte Carlo. (e) and (f) same as (c) and (d) for core KNFa in the time period from 1854-1823.

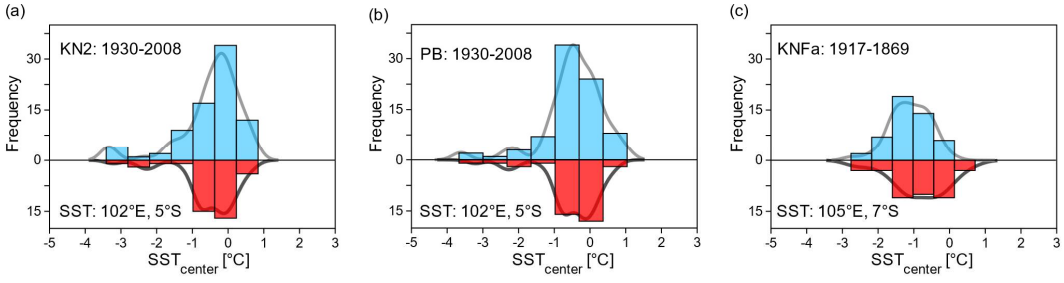

Figure 8: Distribution of August-October mean SST$_{centre}$ inferred from the Enggano Sr/Ca records (in blue) compared to satellite SSTs (in red, OI SST, 1982-2008) (Huang et al., 2021), centered to its mean. Thick grey lines are the Kernel density functions of the histograms. (a, b) Modern SST$_{centre}$ (KN2 and PB) from 2008-1930 shows the same distribution as SSTs in the grid centred at Enggano island. The negative skewness reflects the occurrence of extreme positive IOD events. In the time period of 1917-1855, SST$_{centre}$ (KNFa) shows a symmetric distribution, comparable to the August-September SST distribution seen today at 7°S. Histograms computed using PAST (Hammer et al., 2001).

https://doi.org/10.5194/cp-2024-25
Preprint. Discussion started: 15 April 2024

5.4 Meridional and zonal Indian Ocean SST gradients in historical data

In the satellite era, interannual variations of meridional and zonal SST gradients across the tropical Indian Ocean are coupled, i.e. a northward contraction of the Indian Ocean Warm Pool is typically also associated with a reversal of the zonal SST gradient, resulting in a positive IOD event (Weller and Cai, 2014). To assess this relationship on historical time scales, we have computed meridional and zonal temperature gradients across the tropical Indian Ocean from historical data. We have used HadCRUT5, a dataset that blends SST and surface air temperatures, but does not use spatial interpolation to fill data gaps (Morice et al., 2021), providing the best coverage of actual temperature measurements before 1900. Note, however, that these long-term SST gradients may still be effected by sparse observations in the Indian Ocean prior to the satellite era (Gopika et al., 2020). The zonal SST gradient in the equatorial Indian Ocean shows a long-term increase reflecting the continuous warming of the western Indian Ocean, which appears to have started before the beginning of historical records (Fig. 9) (Roxy et al., 2014; Gopika et al., 2020; Pfeiffer et al., 2017), at rates exceeding eastern Indian Ocean warming (Gopika et al., 2020). The meridional SST gradient, in contrast, does not show a significant long-term trend, but multidecadal variations. It reverses in sign and diverges from the zonal SST gradient prior to 1925, with a warmer north-eastern Indian Ocean relative to the south-eastern tropical Indian Ocean (Fig. 9). In this period, the meridional SST gradient may have even exceeded present-day values. Taken together, this suggests a warmer eastern Indian Ocean (relative to the west) with a stronger north-south meridional SST gradient in the east. Similar results (not shown) where obtained using GISS Surface Temperature data (GISTEMP v4, 250 km smoothing) (Lenssen et al., 2019). Thus, the positive linear relationship between meridional and zonal SST gradients seen on interannual time scales (Weller and Cai, 2014) does not hold on multidecadal periods. The positive north-south SST gradient prior to ~1930 should drive stronger SE winds off Java and Sumatra in austral spring, and shift the mean position of the ITCZ to the north of Enggano Island, supporting our interpretation of the Enggano coral Sr/Ca data.

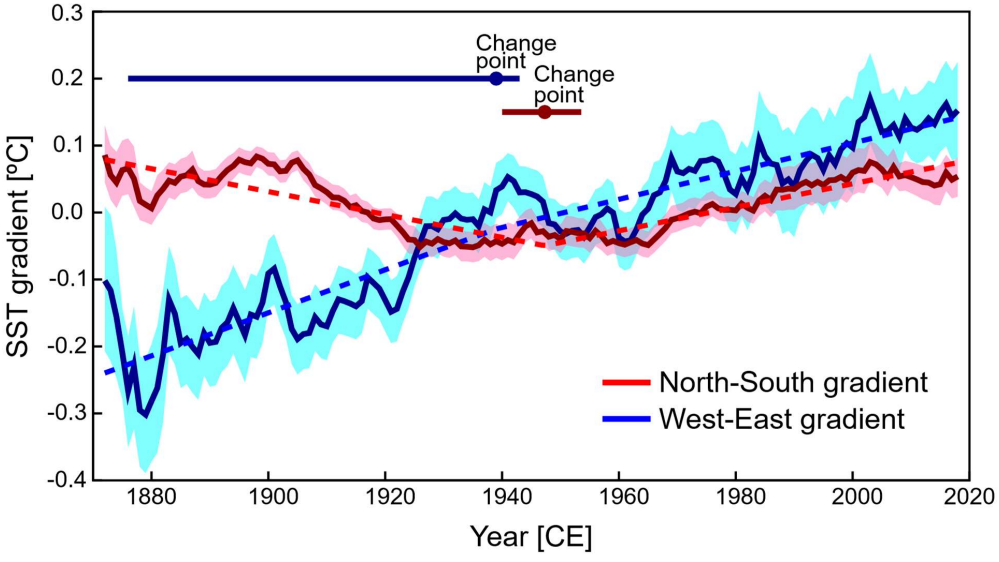

Figure 9: Temperature gradients in the tropical Indian Ocean. North-south (red; 90-110°E, 2.5-7.5°N minus 90-110°E, 10°S-Equator) and west-east (blue; 50-70°E, 10°S-10°N minus 90-110°E, 10°S-Equator) Indian Ocean temperature gradients using HadCRUT5 (Morice et al., 2021). Temperature gradients are smoothed using 21 year moving averages. Pink and blue shades indicate uncertainty (1σ) calculated using bootstrap methods. The west-east Indian Ocean temperature gradient increases steadily since 1880 ($p < 0.01$, Mann-Kendall test), but possibly decelerates after 1939 (95%CI: 1876~1943 CE, SiZer test (Chaudhuri and Marron, 1999), blue horizontal line with circle). The exact onset of the deceleration cannot be determined (not the large 95% confidence levels of the SiZer test). The north-south Indian Ocean temperature gradient does not show a significant long-term trend ($p > 0.1$, Mann-Kendall test) and reverses prior to 1947 (95%CI 1940~1953 CE, red horizontal line with circle).

https://doi.org/10.5194/cp-2024-25
Preprint. Discussion started: 15 April 2024

5.5 Comparison with other proxy records from the SE tropical Indian Ocean

The first coral reconstruction of eastern Indian Ocean climate variability derives from a coral $\delta^{18}O$ record from the northern Mentawai Islands, located approximately 4 ° further north of Enggano Island (Fig. 2, Fig. 3, Fig. A1, Fig. A2) (Abram et al., 2008). The record lies at the northern edge of the Sumatra upwelling zone and extends from 1997 to 1858 (Fig. 10, i.e. it overlaps with the two modern Enggano coral Sr/Ca records and the upper third of the sub-fossil coral KNFa). The northern Mentawai core records the most extreme positive IOD events in 1997, 1994 and 1961, when the ITCZ shifted far northwards, but not the events of 1963 and 1967 that are seen in the modern Enggano Sr/Ca records (Fig. 10). Wind-induced coastal upwelling did not extend that far north during these events (Abram et al., 2015). The northern Mentawai record thus provides constraints on the northward shift in the position of the ITCZ. The northern Mentawai coral record does not show the increase in SST seasonality between 1917 and 1855 seen in the KNFa coral record (Fig. 10), which is attributed to a strengthening of the SE winds off Java and Sumatra in austral spring. This would suggest that the ITCZ did not shift beyond the northern Mentawai Islands in this period. Prior to 1961, the northern Mentawai record shows one extreme positive IOD event in 1877 that coincided with the very strong El Nino of 1877/78 (Abram et al., 2008) . This event caused record drought and famine in much of Asia (Davis, 2002) and strong warming in the western tropical Indian Ocean (Pfeiffer and Dullo, 2006; Charles et al., 1997). The Mentawai record thus suggests that one extreme positive IOD event occurred between 1917 and 1855 which was at least on par with the devastating event of 1997.

Unfortunately, given the age uncertainty of the sub-fossil Enggano coral Sr/Ca record, it is not possible to unequivocally identify this event in core KNFa. At present, extreme positive IOD events, like the one in 1877 recorded at Mentawai, are less pronounced and more difficult to identify at sites south of 7 °S, due to the strong August-October cooling seen there in every year (note that coastal upwelling cools SSTs to ~25 °C at all sites off Java and Sumatra (Fig. 3), so that anomalously strong upwelling is better recorded at sites with weaker seasonal upwelling and warmer mean August-October SSTs). Therefore, it is still difficult to relate the changes in meridional variability inferred from the Enggano corals to zonal variability associated with the IOD.

Another independent source of information on low-frequency climatic changes in the SE tropical Indian Ocean is provided by sediment cores. Their temporal resolution and age control are much lower when compared to sub-fossil coral records, but their record is more continuous and covers longer time periods. Steinke et al. (2014b) investigated a sediment core in the Timor Sea, north-west of Sumba Island (Fig. 11) spanning the last 2000 years. Sumba Island is located south-east of the main upwelling zone off the coast of Java (Fig. 2). In this region, moderate and extreme positive IOD events cause anomalous cooling of SSTs (note that moderate IODs tend to cause even stronger cooling than strong ones) (Fig. A2). A modern coral Sr/Ca record from nearby Timor Island (10 °S, 123 °E), which extends from 2004 to 1914, shows that decadal SST variability in this region tracks decadal IOD variability (Cahyarini et al., 2014). The top of the sediment core from Sumba Island is dated to 1984 ±6 years CE (Steinke et al., 2014a). The record includes mixed layer temperatures inferred from foraminiferal Mg/Ca ratios with a temporal resolution of ~5 years, and relative abundances of mixed layer and thermocline dwelling foraminifers, with a temporal resolution of ~10 years (Fig. 11). Unfortunately, a turbidite limits the overlap with the Enggano Sr/Ca record to 1845 ±9 years BP (Steinke et al., 2014a), which hampers a comparison with the shift back to modern SST seasonality between 1822 and 1854 seen in the coral record. Nevertheless, the sediment core data shows a cooling of SSTs from a mean of 25.0 °C between 1984-1932 to a mean of 23.8 °C between 1928 and 1845, i.e. the difference exceeds -1 °C, which is statistically significant based on a two-sided students t-test ($p>0.05$). The inferred decrease in mean SST is accompanied by an increase of thermocline dwelling foraminifers (Fig. 11). This indicates that a shallowing of the thermocline in the SE tropical Indian Ocean prior to ~1930, favoring increased upwelling of cold water, as the most likely driver of the inferred cooling trend. Steinke et al. (2014) linkedn this decrease in mean SST and thermocline depth to stronger SE trade winds in the SE tropical Indian Ocean, which is fully consistent with our interpretation of the Enggano Sr/Ca record. Furthermore, (Steinke et al., 2014b) suggest that these changes are part of a longer-term trend to cooler temperatures and a shallower thermocline during

https://doi.org/10.5194/cp-2024-25
Preprint. Discussion started: 15 April 2024

the Little Ice Age, despite some modulation by multi-decadal variability. During the medieval warm period, SE Indian Ocean SSTs warmed again and the thermocline deepened, which should have reduced upwelling of cold water off Java and Sumatra (Steinke et al., 2014b). Interestingly, a 40-year sub-fossil coral Sr/Ca record from Lampung Bay, located between Java and Sumatra, suggests reduced seasonal and interannual (IOD) variability during the medieval warm period (Cahyarini et al., 2021), consistent with the record of Steinke et al. (2014b). Thus, the study of Steinke et al. (2014) lends support to the changes in mean climate in the eastern equatorial Indian Ocean inferred from the Enggano Sr/Ca record, and suggests that it may be part of a centennial trend modulated by multi-decadal variability that extends beyond the time period covered by the instrumental and coral record from the SE tropical Indian Ocean.

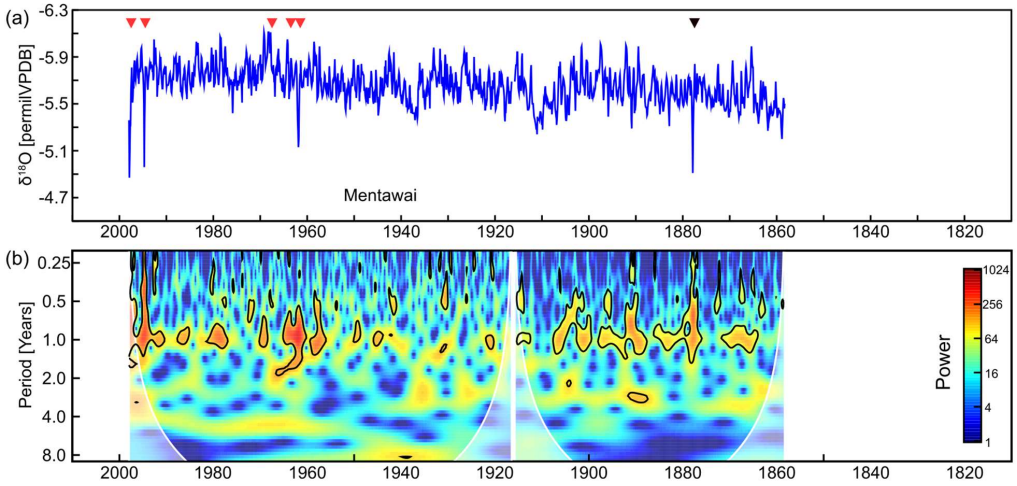

Figure 10: Monthly coral $\delta^{18}O$ record from northern Mentawai from (Abram et al., 2008). (a) monthly mean coral $\delta^{18}O$ (thin blue lines) and ten-year running averages (thick red line) from 1858-1997. The data is scaled so that one tick mark corresponds to 1 °C assuming a coral $\delta^{18}O$-SST relationship of -0.2 permil 1 °C^{-1} (Watanabe and Pfeiffer, 2022). Red arrows mark extreme positive IOD events seen in the Sr/Ca record from Enggano (Pfeiffer et al., 2022). Note: The Mentawai coral record does not record the events of 1963 and 1967. One extreme positive IOD event is recorded in 1877 (black arrow). (b) Wavelet Power spectrum of the Mentawai record, with largest variability on interannual periodicities. Wavelet Power spectrum was computed in R using the Morlet Wavelet.

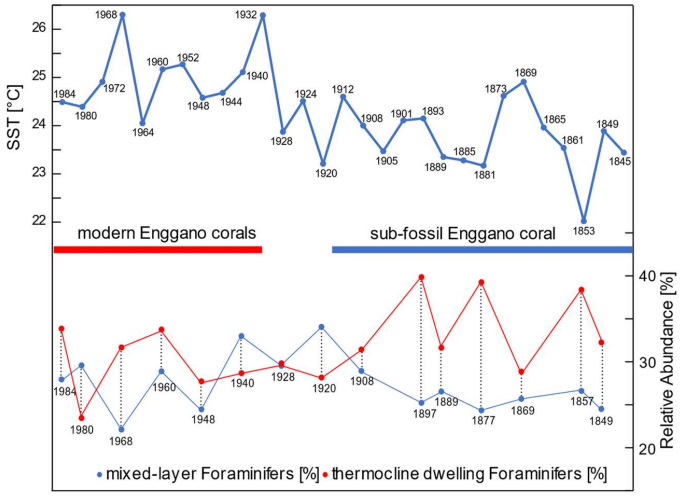

Figure 11. Top: Mean SSTs inferred from Foraminiferal Mg/Ca ratios from a sediment core taken off Sumba Island (Steinke et al., 2014a; Steinke et al., 2014b). Each dot represents one measurement, with estimated ages of Steinke et al. (2014b). Red (blue) horizontal bars indicate time period covered by modern (sub-fossil) coral records from Enggano Island. Bottom: Relative abundance of mixed layer (blue dots) and thermocline dwelling (red dots) foraminifers (Steinke et al., 2014b). See text for discussion.

https://doi.org/10.5194/cp-2024-25
Preprint. Discussion started: 15 April 2024

6 Summary and Conclusions

The Enggano Sr/Ca record reveals changes in SST seasonality in the SE tropical Indian Ocean on historical time scales. A period with enhanced seasonality occurs between 1917 and 1855 due to a cooling of mean August-October SSTs. This indicates an early onset of the Asian summer monsoon coupled with a northward expansion and strengthening of the SE winds of Java and Sumatra, qualitatively consistent with low-frequency, centennial-scale changes inferred from high-resolution sediment core data (Steinke et al., 2014b). We attribute the enhanced seasonality to an enhanced meridional temperature gradient in the eastern tropical Indian Ocean, with warming in the north relative to the south, and a northward shift of the ITCZ. We note that the positive correlation between the meridional and the zonal SST gradient in the tropical Indian Ocean seen on interannual time scales does not hold on multi-decadal time periods. Between 1917 and 1855, the magnitude of the mean August-November cooling at Enggano Island is comparable to the cooling seen today during 'weaker' extreme and moderate positive IOD events. As even moderate IOD events may have significant climatic impacts in Indian Ocean rim countries, this warrants further investigation, especially since our data indicate quite abrupt transitions in seasonality on historical time scales. We conclude that meridional variability in the SE tropical Indian Ocean needs to be better understood. An array approach combining coral proxy data and high-resolution sediment core records along the coasts of Java and Sumatra would be ideal to better capture the full spectrum of climate variability in the SE tropical Indian Ocean.

Author contribution: M.P. conceived the study and wrote the paper. H.T. measured and interpreted the Sr/Ca data, L.R. assessed the preservation of the coral samples. L.R., T.K.W., S.I., D.G.-S. and S.Y.C. contributed to data analysis and interpretation. T.K.W., C.C.W., C.-C.S., J.Z. and G.-J.B. helped dating the samples and with the development of the age models. S.Y.C. selected the study area and led the fieldwork.

Competing interests: The authors declare that they have no competing interests.

Data and materials availability: All methods needed to evaluate the conclusions in the paper are present in the paper and/or the supplementary material. The Sr/Ca will be archived at the Paleoclimatology Branch of NOAA's National Center for Environmental Information (NCEI) (http://www.ncdc.noaa.gov/data-access/paleoclimatology-data) after acceptance of the manuscript. The raw materials are stored at BRIN (Indonesia).

Acknowledgments: We thank Karen Bremer for laboratory assistance and the Deutsche Forschungsgemeinschaft (DFG) for funding the projects 468545728, 260218773 and 39931928. S.Y.C. acknowledges support from the Indonesia Toray Science Foundation Research Grant 2007 and the Alexander von Humboldt Georg Forster Research Fellowship for Experienced Researchers (Ref 3.5 - IDN - 1158893 - GF-E). H.T. and T.W. were supported by the program 'Multiple approaches for understanding earth environmental changes using biogenetic carbonates', Strategic Young Researcher Overseas Visits Program for Accelerating Brain Circulation, Ministry of Education, Culture, Sports, Science and Technology (MEXT), Japan. We acknowledge the Indonesia Government Research Permit No: 46/SIP/IV/FR/5/2022. U/Th dating was supported by grants from the National Taiwan University (NTU) Core Consortiums Project (112L894202), Higher Education Sprout Project of the Ministry of Education (112L901001) and the National Science and Technology Council (111-2116-M-002-022-MY3).

https://doi.org/10.5194/cp-2024-25
Preprint. Discussion started: 15 April 2024

Climate of the Past
Discussions

Appendices

Table A1: Uranium and Thorium isotopic compositions and ^{230}Th ages of core KNFa by MC-ICPMS, Thermo Electron Neptune, at National Taiwan University.

Sample	Weight	^{238}U		^{232}Th		d^{234}U		[^{230}Th/^{238}U]		[^{230}Th/^{232}Th]		Age		Age		$d^{234}U_{initial}$		AD		AD	
ID	g	ppb[a]		ppt		measured[a]		activity[c]		ppm[d]		uncorrected		corrected[c,e]		corrected[b]		uncorrected		corrected	
KNFa(2/11)	0.1785	1870.4	±2.0	2115.3	±5.7	146.2	±1.8	0.001395	±0.000030	20.33	±0.44	132.8	±2.9	107	±13	146.2	±1.8	1,881	±3	1,907	±13
KNFa(3/11)*	0.2028	2553.4	±2.1	494.8	±2.4	143.2	±1.3	0.001241	±0.000013	105.6	±1.2	118.4	±1.3	113.9	±2.6	143.2	±1.3	1,897.1	±1.3	1,901.6	±2.6
KNFa(5/11)	0.1815	1845.4	±1.7	521.5	±2.7	143.1	±1.8	0.001621	±0.000015	94.6	±1.0	154.7	±1.4	148.2	±3.6	143.2	±1.8	1,859.0	±1.4	1,865.5	±3.6
KNFa(7/11)*	0.2011	2565.9	±2.1	330.6	±2.3	143.8	±1.2	0.001713	±0.000013	219.2	±2.2	163.4	±1.2	160.4	±1.9	143.8	±1.2	1,852.1	±1.2	1,855.1	±1.9
KNFa(8/11)	0.2092	1842.3	±2.2	224.9	±2.2	144.9	±1.6	0.001658	±0.000011	223.9	±2.7	158.0	±1.1	155.2	±1.8	144.9	±1.6	1,855.7	±1.1	1,858.5	±1.8
KNFa(10/11)	0.1965	1791.0	±2.0	260.4	±2.4	145.7	±1.7	0.001923	±0.000014	218.2	±2.6	183.2	±1.4	179.9	±2.2	145.7	±1.7	1,830.5	±1.4	1,833.8	±2.2

Analytical errors are 2σ of the mean

[a]$[^{238}U] = [^{235}U] \times 137.77$ (±0.11‰) for marine samples (Hiess et al., 2012); $\delta^{234}U = ([^{234}U/^{238}U]_{activity} - 1) \times 1000$

[b]$\delta^{234}U_{initial}$ corrected was calculated based on ^{230}Th age (T), i.e., $\delta^{234}U_{initial} = \delta^{234}U_{measured}\, X\, e^{\lambda 234 * T}$, and T is corrected age.

[c]$[^{230}Th/^{238}U]_{activity} = 1 - e^{-\lambda 230 T} + (\delta^{234}U_{measured}/1000)[\lambda_{230}/(\lambda_{230} - \lambda_{234})](1 - e^{-(\lambda 230 - \lambda 234)\, T})$, where T is the age.

Decay constants are 9.1705×10^{-6} yr^{-1} for ^{230}Th, 2.8221×10^{-6} yr^{-1} for ^{234}U (Cheng et al., 2012), and 1.55125×10^{-10} yr^{-1} for ^{238}U (Jaffey et al., 1971)

[d]The degree of detrital ^{230}Th contamination is indicated by the [^{230}Th/^{232}Th] atomic ratio instead of the activity ratio.

[e]Age corrections for samples were calculated using an estimated atomic ^{230}Th/^{232}Th ratio of 4 ± 2 ppm (Shen et al., 2008).

https://doi.org/10.5194/cp-2024-25
Preprint. Discussion started: 15 April 2024

Figure A1: Evolution of coastal upwelling off Java and Sumatra in austral spring (June-November) as expressed in the standard deviation of monthly mean SST (colors). Coastal upwelling starts off Java in June, strengthens in July and spreads to southern Sumatra in July/August. In September/October, upwelling reaches the Mentawai islands located between 3° S and the equator. Coastal upwelling subsides in November. Arrows mark position of Enggano (E) and Mentawai (M). Charts were computed at the knmi climate explorer (https://climexp.knmi.nl)

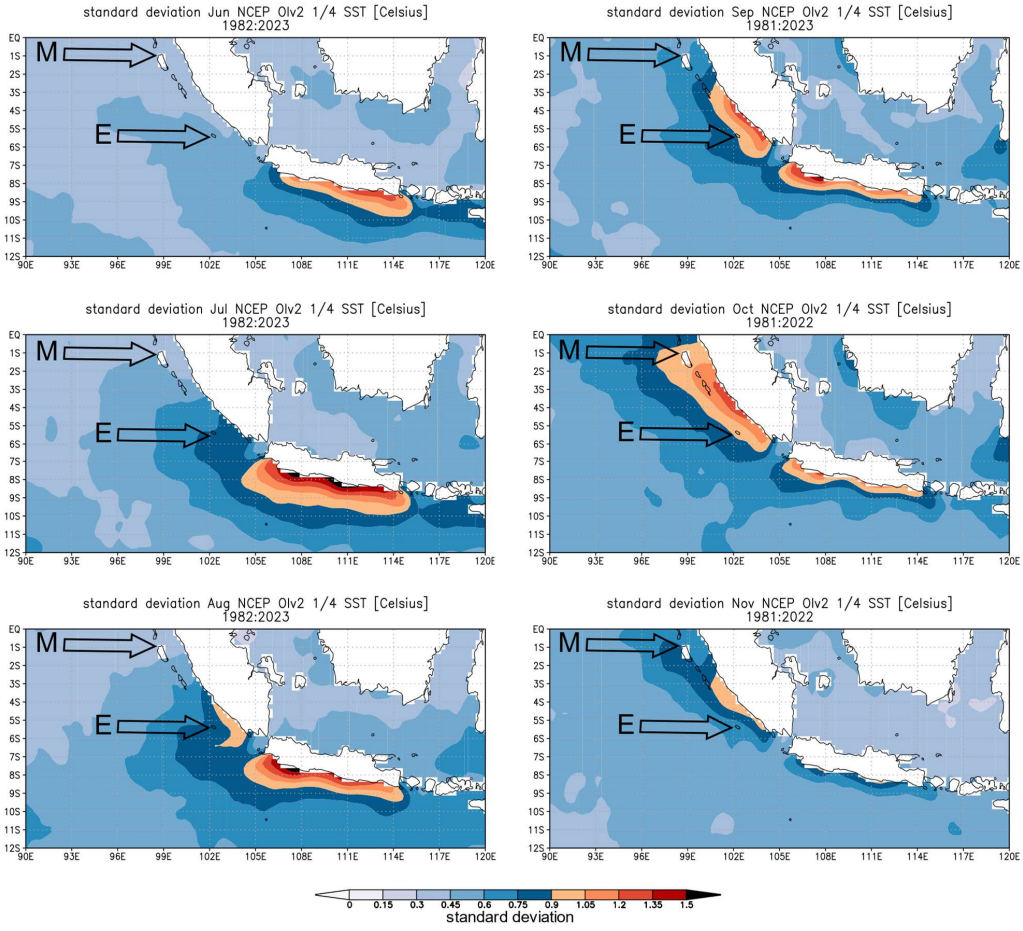

https://doi.org/10.5194/cp-2024-25
Preprint. Discussion started: 15 April 2024

Figure A2: Composite maps of August-November SST anomalies during (a) extreme positive IOD events (2019, 2006, 1997, 1994) and (b) moderate positive IOD events (2015, 2012, 1982, 1983). Arrows mark position of Enggano (E), Mentawai (M) and Sumba (S). Data from AVHRR-OI SST (1/4° grids, 1982-2022) (Huang et al., 2021). Charts computed at https://iridl.ldeo.columbia.edu/.

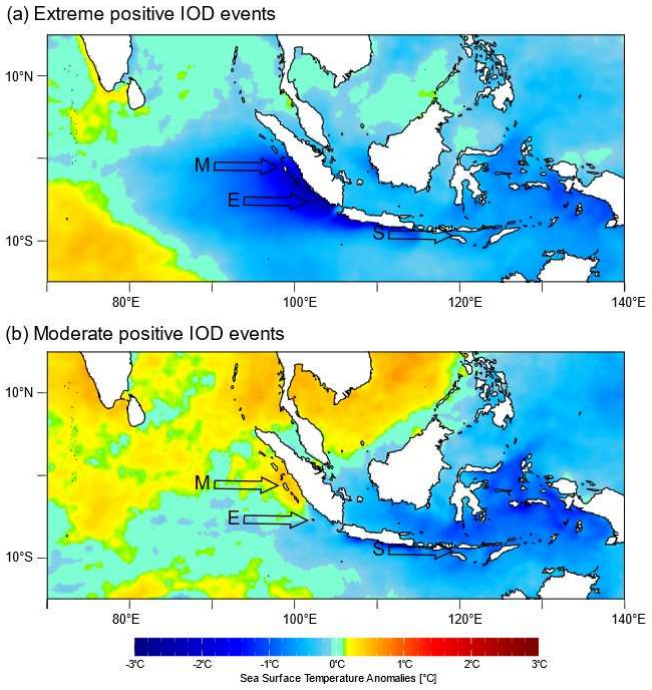

Figure A3: Luminescence scan of the sub-fossil coral core KNFa from Enggano. Core slabs are numbered. Note the dull, mottled appearance of the core top, which extends to the top of slab 2 and indicates potential secondary alteration. Parts of slab 6 look similar, although the effect is not as pronounced. These parts and adjacent transects were investigated using the Hitachi SU3900 Scanning electron microscope (SEM) with extra-large chamber. Slab 10 and 11 show localized alterations which occur in areas affected by bioerosion.

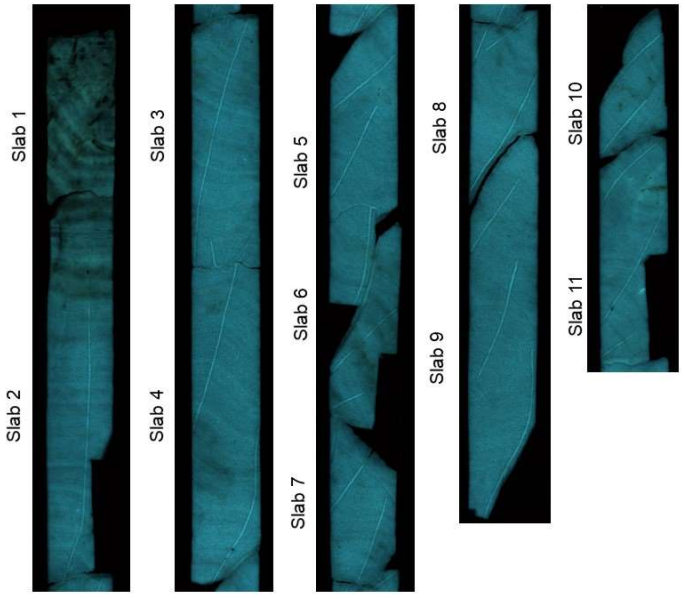

https://doi.org/10.5194/cp-2024-25
Preprint. Discussion started: 15 April 2024

Figure A4: Hitachi SU3900 Scanning electron microscope with extra-large chamber. The sample holder has a diameter of 28 cm, shown here with slab 6 of core KNFa.

Figure A5: Scanning electron microscopy images showing pristine and diagenetic altered parts of sub-fossil coral KNFa. The top 14 cm of the core shows several macroscopic bioerosion traces on x-ray images (Fig. 4). This interval (a and b) is characterized by filamentous microborings (MB), dissolution (D) of centers of calcification and secondary aragonite (SA) cement. The degree of cementation is variable, ranging from (a) pristine coral skeletons and traces of cement to (b) more pervasive fibrous aragonite cement (5 to 10 µm-length). The interval below 14 cm is generally pristine (c) showing smooth primary aragonite (PA) skeletal surfaces. The only exception occurs in an interval from the base of slab 5 to the top of slab 7 (Fig. 5). A patch of secondary aragonite cement on transect 10 of slab 6 caused an extreme spike in the proxy record with unusually low Sr/Ca ratio of 9.32 mmol/mol. This 'false alarm' spike escaped detection by our first standard diagenetic screening, but was identified by our semi contentious SEM screening along the proxy sampling track.

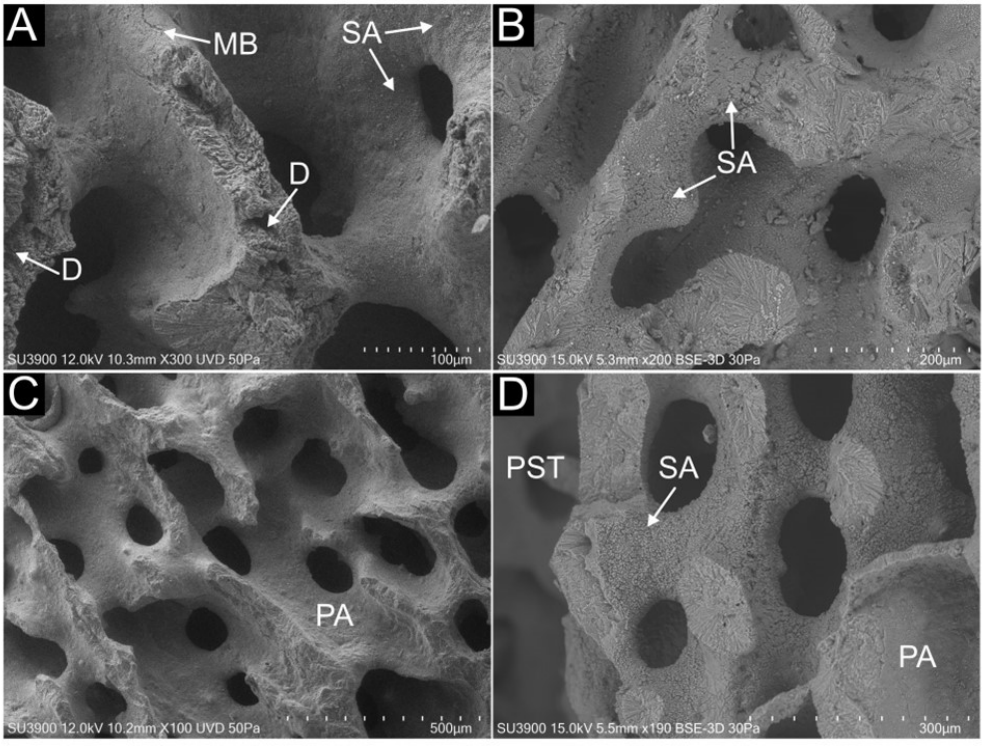

https://doi.org/10.5194/cp-2024-25
Preprint. Discussion started: 15 April 2024

Figure A6: Corrected U/Th ages of core KNFa with 2σ uncertainties vs. the number of years estimated from seasonal cycles in coral Sr/Ca. The oldest year of KNFa is year 1. The age of the coral core was estimated from the intercept of the linear regression between the U/Th ages and the annual cycles of Sr/Ca (Fig. 5), assuming that the slope of this regression is one (i.e. assuming that the U/Th ages agree with the number of annual cycles seen in coral Sr/Ca) (Domínguez-Villar et al., 2012). The base of KNFa is dated to 1823 ± 2.4 (2σ). The floating age uncertainty was estimated with a Monte Carlo approach (20,000 loops) using the 2σ U/Th error.

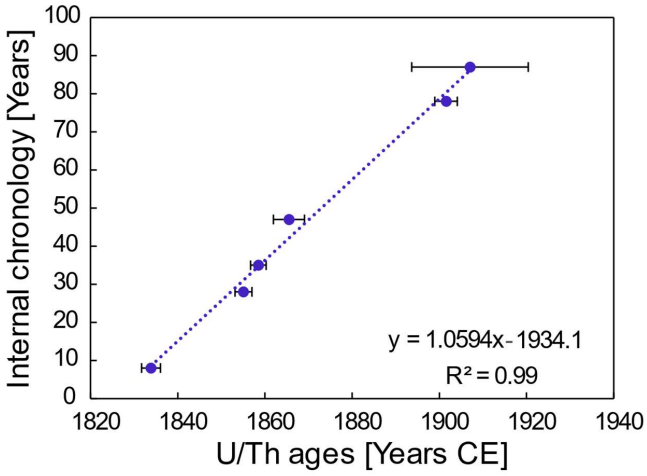

Figure A7: Violin and boxplots showing the distribution of monthly mean SSTs inferred from the modern Enggano corals (PB, KN2) compared with satellite SST (OI SST, ¼° grid) from 2008-1982 (Huang et al., 2021). Coral Sr/Ca has been centered to its mean and converted to SST assuming a Sr/Ca-SST relationship of -0.06 mmol mol^{-1} 1 °C^{-1}. Open circles (stars) indicate outliers exceeding ±1 (±1.5) standard deviations of the interquartile range. Violin plots computed using PAST (Hammer et al., 2001).

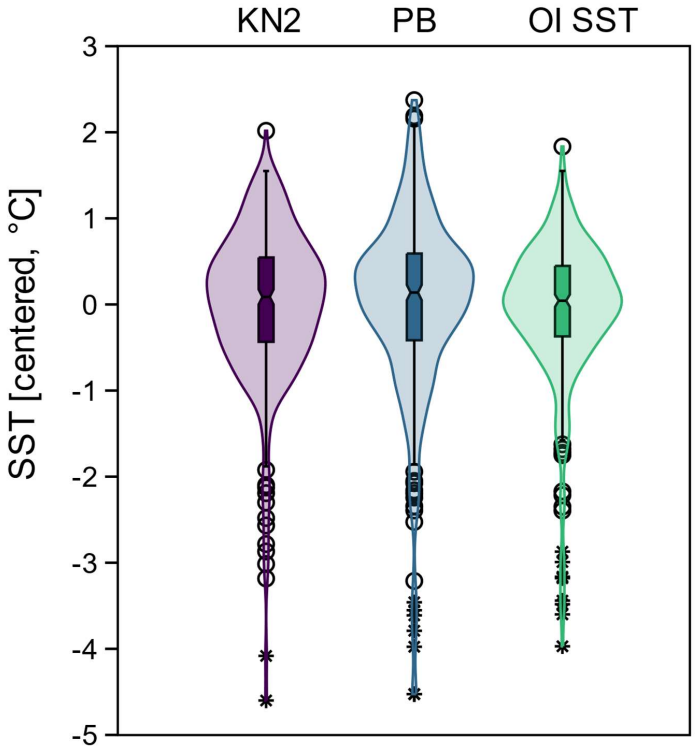

https://doi.org/10.5194/cp-2024-25
Preprint. Discussion started: 15 April 2024

Figure A8: Modern and sub-fossil, monthly interpolated coral Sr/Ca time series from Enggano. (a) The complete Enggano Sr/Ca record comprises two modern (PB, KN2) and one sub-fossil core (KNFa) and extends from 2008-1930, 1917-1869 and 1861-1823. Thin blue and green lines are monthly data, thick red solid and dashed lines are 10-year running means. Note that the sub-fossil record has a floating chronology based on U/Th dating with an age uncertainty of ± 2.4 years (2σ). Relative changes in Sr/Ca reflect temperature variations with a mean Sr/Ca-SST relationship of -0.06 mmol mol 1 °C^{-1} (Watanabe and Pfeiffer, 2022), which corresponds to one tick mark on the y-axis. Positive Sr/Ca anomalies in 2006,1997,1994, 1967, 1963 and 1961 indicate extreme positive IOD events (red arrows). The sub-fossil record from KNFa indicates an extreme positive IOD event in ~1825 (black arrow). Events in 1907 and 1916 may be comparable with the comparatively weaker, but still extreme positive IOD of 2006. (b) and (c) distribution of monthly coral Sr/Ca data in ~20-year bins shown as violin and boxplots. Values >1 standard deviation (>1.5 standard deviations) above or below the 1.5 % interquartile range are plotted as open circles (stars). Outliers reflect extreme positive IOD events. (a) Cores PB and KN2, 2008-1930. The Sr/Ca distributions are negatively skewed in 2008-1990 and 1969-1950 due to the occurrence of extreme positive IOD events. Note the consistent shift in the medians of PB and KN2 Sr/Ca data, indicating that vital effects remained stable over time. (c) Data from KNFa shows a symmetric distribution between 1917-1855, with a larger spread around the median and few outliers. Between 1854 and 1923, the Sr/Ca distribution is comparable to modern values. Violin plots computed using PAST (Hammer et al., 2001).

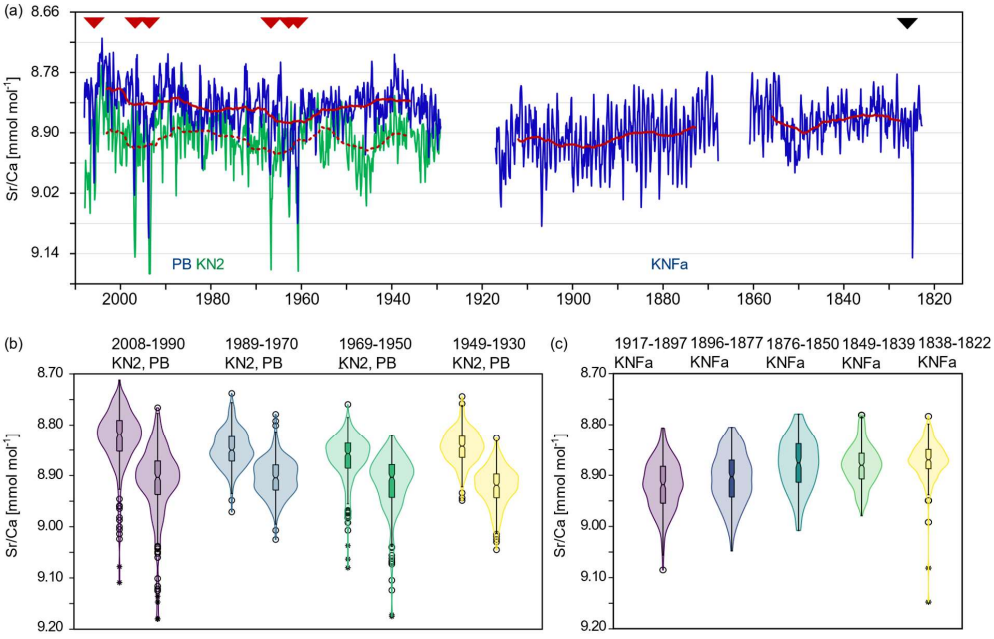

https://doi.org/10.5194/cp-2024-25
Preprint. Discussion started: 15 April 2024

Figure A9: Temperature gradients in the tropical Indian Ocean. (a) North-south SST gradient in the eastern Indian Ocean calculated from satellite SST (OI SST, ¼° grid, available since 1982) (Huang et al., 2021) compared with mean August-October SST_{centre} inferred from KN2 and PB. (b) Linear regression of August-October SST_{centre} inferred from core PB and North-South SST gradient. (c) Same as (b) but for core KN2. SST_{centre} correlates negatively with the meridional SST gradient (colder SSTs at Enggano Island correspond to a stronger meridional SST gradient).

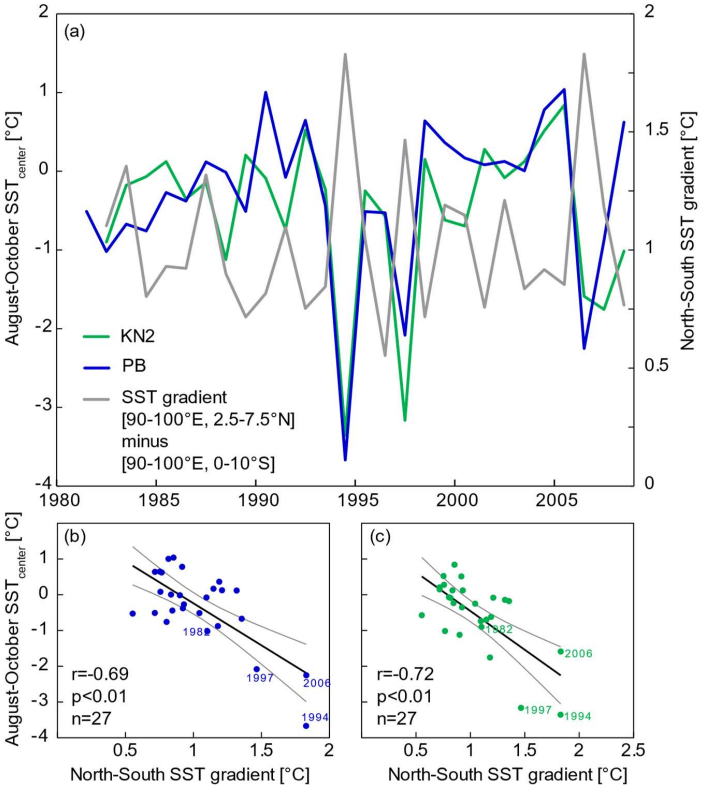

https://doi.org/10.5194/cp-2024-25
Preprint. Discussion started: 15 April 2024

References

Abram, N. J., Dixon, B. C., Rosevear, M. G., Plunkett, B., Gagan, M. K., Hantoro, W. S., and Phipps, S. J.: Optimized coral reconstructions of the Indian Ocean Dipole: An assessment of location and length considerations, Paleoceanography, 30, 1391–1405, doi:10.1002/2015PA002810, 2015.

Abram, N. J., Gagan, M. K., Cole, J. E., Hantoro, W. S., and Mudelsee, M.: Recent intensification of tropical climate variability in the Indian Ocean, Nat. Geosci., 1, 849–853, doi:10.1038/ngeo357, 2008.

Abram, N. J., Gagan, M. K., Liu, Z., Hantoro, W. S., McCulloch, M. T., and Suwargadi, B. W.: Seasonal characteristics of the Indian Ocean Dipole during the Holocene epoch, Nature, 445, 299–302, doi:10.1038/nature05477, 2007.

Abram, N. J., Gagan, M. K., McCulloch, M. T., Chappell, J., and Hantoro, W. S.: Coral reef death during the 1997 Indian Ocean Dipole linked to Indonesian wildfires, Science (New York, N.Y.), 301, 952–955, doi:10.1126/science.1083841, 2003.

Abram, N. J., Wright, N. M., Ellis, B., Dixon, B. C., Wurtzel, J. B., England, M. H., Ummenhofer, C. C., Philibosian, B., Cahyarini, S. Y., Yu, T.-L., Shen, C.-C., Cheng, H., Edwards, R. L., and Heslop, D.: Coupling of Indo-Pacific climate variability over the last millennium, Nature, 579, 385–392, doi:10.1038/s41586-020-2084-4, 2020.

Allison, N., Finch, A. A., Webster, J. M., and Clague, D. A.: Palaeoenvironmental records from fossil corals: The effects of submarine diagenesis on temperature and climate estimates, Geochimica et Cosmochimica Acta, 71, 4693–4703, doi:10.1016/j.gca.2007.07.026, 2007.

Ashok, K., Guan, Z., and Yamagata, T.: Influence of the Indian Ocean Dipole on the Australian winter rainfall, Geophysical Research Letters, 30, doi:10.1029/2003GL017926, 2003.

Behera, S. K., Luo, J.-J., Masson, S., Delecluse, P., Gualdi, S., Navarra, A., and Yamagata, T.: Paramount Impact of the Indian Ocean Dipole on the East African Short Rains: A CGCM Study, J. Climate, 18, 4514–4530, doi:10.1175/JCLI3541.1, 2005.

Cahyarini, S. Y., Pfeiffer, M., Dullo, W.-C., Zinke, J., Hetzinger, S., Kasper, S., Grove, C., and Garbe-Schönberg, D.: Comment on "A snapshot of climate variability at Tahiti at 9.5 ka using a fossil coral from IODP Expedition 310" by Kristine L. DeLong, Terrence M. Quinn, Chuan-Chou Shen, and Ke Lin, Geochem. Geophys. Geosyst., 12, n/a-n/a, doi:10.1029/2010GC003377, 2011.

Cahyarini, S. Y., Pfeiffer, M., Nurhati, I. S., Aldrian, E., Dullo, W.-C., and Hetzinger, S.: Twentieth century sea surface temperature and salinity variations at Timor inferred from paired coral δ 18 O and Sr/Ca measurements, Journal of Geophysical Research: Oceans, 119, 4593–4604, doi:10.1002/2013jc009594, 2014a.

Cahyarini, S. Y., Pfeiffer, M., Nurhati, I. S., Aldrian, E., Dullo, W.-C., and Hetzinger, S.: Twentieth century sea surface temperature and salinity variations at Timor inferred from paired coral δ 18 O and Sr/Ca measurements, J. Geophys. Res. Oceans, 119, 4593–4604, doi:10.1002/2013JC009594, 2014b.

Cahyarini, S. Y., Pfeiffer, M., Reuning, L., Liebetrau, V., Dullo, W.-C., Takayanagi, H., Anwar, I. P., Utami, D. A., Garbe-Schönberg, D., Hendrizan, M., and Eisenhauer, A.: Modern and sub-fossil corals suggest reduced temperature variability in the eastern pole of the Indian Ocean Dipole during the medieval climate anomaly, Scientific reports, 11, 14952, doi:10.1038/s41598-021-94465-1, 2021.

Cai, W., Zheng, X.-T., Weller, E., Collins, M., Cowan, T., Lengaigne, M., Yu, W., and Yamagata, T.: Projected response of the Indian Ocean Dipole to greenhouse warming, Nat. Geosci., 6, 999–1007, doi:10.1038/ngeo2009, 2013.

Charles, C. D., Hunter, D. E., and Fairbanks, R. G.: Interaction Between the ENSO and the Asian Monsoon in a Coral Record of Tropical Climate, Science (New York, N.Y.), 277, 925–928, doi:10.1126/science.277.5328.925, 1997.

Chaudhuri, P. and Marron, J. S.: SiZer for Exploration of Structures in Curves, Journal of the American Statistical Association, 94, 807–823, doi:10.1080/01621459.1999.10474186, 1999.

https://doi.org/10.5194/cp-2024-25
Preprint. Discussion started: 15 April 2024

Cobb, K. M., Westphal, N., Sayani, H. R., Watson, J. T., Di Lorenzo, E., Cheng, H., Edwards, R. L., and Charles, C. D.: Highly variable El Niño-Southern Oscillation throughout the Holocene, Science (New York, N.Y.), 339, 67–70, doi:10.1126/science.1228246, 2013.

Corrège, T.: Sea surface temperature and salinity reconstruction from coral geochemical tracers, Palaeogeography, Palaeoclimatology, Palaeoecology, 232, 408–428, doi:10.1016/j.palaeo.2005.10.014, 2006.

Davis, M.: Late Victorian holocausts: El Niño famines and the making of the third world, ACLS Humanities E-Book, Verso, London, 464 pp., 2002.

DeLong, K. L., Quinn, T. M., Taylor, F. W., Shen, C.-C., and Lin, K.: Improving coral-base paleoclimate reconstructions by replicating 350years of coral Sr/Ca variations, Palaeogeography, Palaeoclimatology, Palaeoecology, 373, 6–24, doi:10.1016/j.palaeo.2012.08.019, 2013.

Domínguez-Villar, D., Baker, A., Fairchild, I. J., and Edwards, R. L.: A method to anchor floating chronologies in annually laminated speleothems with U–Th dates, Quaternary Geochronology, 14, 57–66, doi:10.1016/j.quageo.2012.04.019, 2012.

Enmar, R., Stein, M., Bar-Matthews, M., Sass, E., Katz, A., and Lazar, B.: Diagenesis in live corals from the Gulf of Aqaba. I. The effect on paleo-oceanography tracers, Geochimica et Cosmochimica Acta, 64, 3123–3132, doi:10.1016/S0016-7037(00)00417-8, 2000.

Fischer, A. S., Terray, P., Guilyardi, E., Gualdi, S., and Delecluse, P.: Two Independent Triggers for the Indian Ocean Dipole/Zonal Mode in a Coupled GCM, J. Climate, 18, 3428–3449, doi:10.1175/JCLI3478.1, 2005.

Gopika, S., Izumo, T., Vialard, J., Lengaigne, M., Suresh, I., and Kumar, M. R. R.: Aliasing of the Indian Ocean externally-forced warming spatial pattern by internal climate variability, Clim Dyn, 54, 1093–1111, doi:10.1007/s00382-019-05049-9, 2020.

Hathorne, E. C., Gagnon, A., Felis, T., Adkins, J., Asami, R., Boer, W., Caillon, N., Case, D., Cobb, K. M., Douville, E., deMenocal, P., Eisenhauer, A., Garbe-Schönberg, D., Geibert, W., Goldstein, S., Hughen, K., Inoue, M., Kawahata, H., Kölling, M., Cornec, F. L., Linsley, B. K., McGregor, H. V., Montagna, P., Nurhati, I. S., Quinn, T. M., Raddatz, J., Rebaubier, H., Robinson, L., Sadekov, A., Sherrell, R., Sinclair, D., Tudhope, A. W., Wei, G., Wong, H., Wu, H. C., and You, C.-F.: Interlaboratory study for coral Sr/Ca and other element/Ca ratio measurements, Geochem. Geophys. Geosyst., 14, 3730–3750, doi:10.1002/ggge.20230, 2013.

Hendy, E. J., Gagan, M. K., Lough, J. M., McCulloch, M., and deMenocal, P. B.: Impact of skeletal dissolution and secondary aragonite on trace element and isotopic climate proxies in Porites corals, Paleoceanography, 22, doi:10.1029/2007PA001462, 2007.

Huang, B., Liu, C., Banzon, V., Freeman, E., Graham, G., Hankins, B., Smith, T., and Zhang, H.-M.: Improvements of the Daily Optimum Interpolation Sea Surface Temperature (DOISST) Version 2.1, Journal of Climate, 34, 2923–2939, doi:10.1175/JCLI-D-20-0166.1, 2021.

Kalnay, E., Kanamitsu, M., Kistler, R., Collins, W., Deaven, D., Gandin, L., Iredell, M., Saha, S., White, G., Woollen, J., Zhu, Y., Leetmaa, A., Reynolds, R., Chelliah, M., Ebisuzaki, W., Higgins, W., Janowiak, J., Mo, K. C., Ropelewski, C., Wang, J., Jenne, R., and Joseph, D.: The NCEP/NCAR 40-Year Reanalysis Project, Bulletin of the American Meteorological Society, 77, 437–471, doi:10.1175/1520-0477(1996)077<0437:TNYRP>2.0.CO;2, 1996.

Lenssen, N. J. L., Schmidt, G. A., Hansen, J. E., Menne, M. J., Persin, A., Ruedy, R., and Zyss, D.: Improvements in the GISTEMP Uncertainty Model, Geophys Res Atmos, 124, 6307–6326, doi:10.1029/2018JD029522, 2019.

Leupold, M., Pfeiffer, M., Garbe-Schönberg, D., and Sheppard, C.: Reef-Scale-Dependent Response of Massive Porites Corals From the Central Indian Ocean to Prolonged Thermal Stress: Evidence From Coral Sr/Ca Measurements, Geochem. Geophys. Geosyst., 20, 1468–1484, doi:10.1029/2018gc007796, 2019.

Leupold, M., Pfeiffer, M., Watanabe, T. K., Reuning, L., Garbe-Schönberg, D., Shen, C.-C., and Brummer, G.-J. A.: El Niño–Southern Oscillation and internal sea surface temperature variability in the tropical Indian Ocean since 1675, Clim. Past, 17, 151–170, doi:10.5194/cp-17-151-2021, 2021.

Linsley, B. K., Wellington, G. M., and Schrag, D. P.: Decadal sea surface temperature variability in the subtropical South Pacific from 1726 to 1997 A.D, Science (New York, N.Y.), 290, 1145–1148, doi:10.1126/science.290.5494.1145, 2000.

McGregor, H. V. and Abram, N. J.: Images of diagenetic textures in Porites corals from Papua New Guinea and Indonesia, Geochem. Geophys. Geosyst., 9, doi:10.1029/2008GC002093, 2008.

Morice, C. P., Kennedy, J. J., Rayner, N. A., Winn, J. P., Hogan, E., Killick, R. E., Dunn, R. J. H., Osborn, T. J., Jones, P. D., and Simpson, I. R.: An Updated Assessment of Near-Surface Temperature Change From 1850: The HadCRUT5 Data Set, Geophys Res Atmos, 126, doi:10.1029/2019JD032361, 2021.

Murphy, R. J., Webster, J. M., Nothdurft, L., Dechnik, B., McGregor, H. V., Patterson, M. A., Sanborn, K. L., Webb, G. E., Kearney, L. I., Rintoul, L., and Erler, D. V.: High-resolution hyperspectral imaging of diagenesis and clays in fossil coral reef material: a nondestructive tool for improving environmental and climate reconstructions, Geochem. Geophys. Geosyst., 18, 3209–3230, doi:10.1002/2017GC006949, 2017.

Newcomb, K. R. and McCann, W. R.: Seismic history and seismotectonics of the Sunda Arc, J. Geophys. Res., 92, 421–439, doi:10.1029/JB092iB01p00421, 1987.

Ng, B., Cai, W., Walsh, K., and Santoso, A.: Nonlinear processes reinforce extreme Indian Ocean Dipole events, Scientific reports, 5, 11697, doi:10.1038/srep11697, 2015.

PAST: Paleontological Statistics Software Package for Education and Data Analysis: http://palaeo-electronica.org/2001_1/past/issue1_01.htm.

Pfeiffer, M. and Dullo, W.-C.: Monsoon-induced cooling of the western equatorial Indian Ocean as recorded in coral oxygen isotope records from the Seychelles covering the period of 1840–1994AD, Quaternary Science Reviews, 25, 993–1009, doi:10.1016/j.quascirev.2005.11.005, 2006.

Pfeiffer, M., Watanabe, T. K., Takayanagi, H., Cahyarini, S. Y., Garbe-Schönberg, D., and Watanabe, T.: Coral Sr/Ca records provide realistic representation of eastern Indian Ocean cooling during extreme positive Indian Ocean Dipole events, Scientific reports, 12, 10642, doi:10.1038/s41598-022-14617-9, 2022.

Pfeiffer, M., Zinke, J., Dullo, W.-C., Garbe-Schönberg, D., Latif, M., and Weber, M. E.: Indian Ocean corals reveal crucial role of World War II bias for twentieth century warming estimates, Scientific reports, 7, 14434, doi:10.1038/s41598-017-14352-6, 2017.

Quinn, T. M. and Taylor, F. W.: SST artifacts in coral proxy records produced by early marine diagenesis in a modern coral from Rabaul, Papua New Guinea, Geophysical Research Letters, 33, doi:10.1029/2005GL024972, 2006.

Reynolds, R. W., Rayner, N. A., Smith, T. M., Stokes, D. C., and Wang, W.: An Improved In Situ and Satellite SST Analysis for Climate, J. Climate, 15, 1609–1625, doi:10.1175/1520-0442(2002)015%3C1609:AIISAS%3E2.0.CO;2, 2002.

Ross, C. L., DeCarlo, T. M., and McCulloch, M. T.: Calibration of Sr/Ca, Li/Mg and Sr-U Paleothermometry in Branching and Foliose Corals, Paleoceanography and Paleoclimatology, 34, 1271–1291, doi:10.1029/2018pa003426, 2019.

Roxy, M. K., Ritika, K., Terray, P., and Masson, S.: The Curious Case of Indian Ocean Warming*,+, Journal of Climate, 27, 8501–8509, doi:10.1175/JCLI-D-14-00471.1, 2014.

Saji, N. H., Goswami, B. N., Vinayachandran, P. N., and Yamagata, T.: A dipole mode in the tropical Indian Ocean, Nature, 401, 360–363, doi:10.1038/43854, 1999.

Saji, N. H. and Yamagata, T.: Possible impacts of Indian Ocean Dipole mode events on global climate, Clim. Res., 25, 151–169, doi:10.3354/cr025151, 2003.

https://doi.org/10.5194/cp-2024-25
Preprint. Discussion started: 15 April 2024

Sanchez, S. C., Westphal, N., Haug, G. H., Cheng, H., Edwards, R. L., Schneider, T., Cobb, K. M., and Charles, C. D.: A Continuous Record of Central Tropical Pacific Climate Since the Midnineteenth Century Reconstructed From Fanning and Palmyra Island Corals: A Case Study in Coral Data Reanalysis, Paleoceanography and Paleoclimatology, 35, doi:10.1029/2020PA003848, 2020.

Sayani, H. R., Cobb, K. M., Cohen, A. L., Elliott, W. C., Nurhati, I. S., Dunbar, R. B., Rose, K. A., and Zaunbrecher, L. K.: Effects of diagenesis on paleoclimate reconstructions from modern and young fossil corals, Geochimica et Cosmochimica Acta, 75, 6361–6373, doi:10.1016/j.gca.2011.08.026, 2011.

Sayani, H. R., Cobb, K. M., Monteleone, B., and Bridges, H.: Accuracy and Reproducibility of Coral Sr/Ca SIMS Timeseries in Modern and Fossil Corals, Geochem. Geophys. Geosyst., 23, doi:10.1029/2021GC010068, 2022.

Schott, F. A., Xie, S.-P., and McCreary, J. P.: Indian Ocean circulation and climate variability, Reviews of Geophysics, 47, doi:10.1029/2007RG000245, 2009.

Schrag, D. P.: Rapid analysis of high-precision Sr/Ca ratios in corals and other marine carbonates, Paleoceanography, 14, 97–102, doi:10.1029/1998PA900025, 1999.

Schreck, C., Lee, H.-T., and Knapp, K.: HIRS Outgoing Longwave Radiation—Daily Climate Data Record: Application toward Identifying Tropical Subseasonal Variability, Remote Sensing, 10, 1325, doi:10.3390/rs10091325, 2018.

Shen, C.-C., Wu, C.-C., Cheng, H., Lawrence Edwards, R., Hsieh, Y.-T., Gallet, S., Chang, C.-C., Li, T.-Y., Lam, D. D., Kano, A., Hori, M., and Spötl, C.: High-precision and high-resolution carbonate 230Th dating by MC-ICP-MS with SEM protocols, Geochimica et Cosmochimica Acta, 99, 71–86, doi:10.1016/j.gca.2012.09.018, 2012.

Smodej, J., Reuning, L., Wollenberg, U., Zinke, J., Pfeiffer, M., and Kukla, P. A.: Two-dimensional X-ray diffraction as a tool for the rapid, nondestructive detection of low calcite quantities in aragonitic corals, Geochem. Geophys. Geosyst., 16, 3778–3788, doi:10.1002/2015GC006009, 2015.

Steinke, S., Mohtadi, M., Prange, M., Varma, V., Pittauerova, D., and Fischer, H. W.: Mid- to Late-Holocene Australian–Indonesian summer monsoon variability, Quaternary Science Reviews, 93, 142–154, doi:10.1016/j.quascirev.2014.04.006, 2014a.

Steinke, S., Prange, M., Feist, C., Groeneveld, J., and Mohtadi, M.: Upwelling variability off southern Indonesia over the past two millennia, Geophysical Research Letters, 41, 7684–7693, doi:10.1002/2014GL061450, 2014b.

Susanto, R. D., Gordon, A. L., and Zheng, Q.: Upwelling along the coasts of Java and Sumatra and its relation to ENSO, Geophys. Res. Lett., 28, 1599–1602, doi:10.1029/2000GL011844, 2001.

Ummenhofer, C. C., England, M. H., McIntosh, P. C., Meyers, G. A., Pook, M. J., Risbey, J. S., Gupta, A. S., and Taschetto, A. S.: What causes southeast Australia's worst droughts?, Geophys. Res. Lett., 36, doi:10.1029/2008GL036801, 2009a.

Ummenhofer, C. C., Sen Gupta, A., England, M. H., and Reason, C. J. C.: Contributions of Indian Ocean Sea Surface Temperatures to Enhanced East African Rainfall, J. Climate, 22, 993–1013, doi:10.1175/2008JCLI2493.1, 2009b.

Villiers, S. de, Greaves, M., and Elderfield, H.: An intensity ratio calibration method for the accurate determination of Mg/Ca and Sr/Ca of marine carbonates by ICP-AES, Geochem. Geophys. Geosyst., 3, doi:10.1029/2001GC000169, 2002.

Villiers, S. de, Shen, G. T., and Nelson, B. K.: The -temperature relationship in coralline aragonite: Influence of variability in and skeletal growth parameters, Geochimica et Cosmochimica Acta, 58, 197–208, doi:10.1016/0016-7037(94)90457-x, 1994.

Watanabe, T. K. and Pfeiffer, M.: A Simple Monte Carlo Approach to Estimate the Uncertainties of SST and δ 18 O sw Inferred From Coral Proxies, Geochem. Geophys. Geosyst., 23, doi:10.1029/2021GC009813, 2022.

Webster, P. J., Moore, A. M., Loschnigg, J. P., and Leben, R. R.: Coupled ocean-atmosphere dynamics in the Indian Ocean during 1997-98, Nature, 401, 356–360, doi:10.1038/43848, 1999.

https://doi.org/10.5194/cp-2024-25
Preprint. Discussion started: 15 April 2024

Weller, E. and Cai, W.: Meridional variability of atmospheric convection associated with the Indian Ocean Dipole Mode, Scientific reports, 4, 3590, doi:10.1038/srep03590, 2014.

Weller, E., Cai, W., Min, S.-K., Wu, L., Ashok, K., and Yamagata, T.: More-frequent extreme northward shifts of eastern Indian Ocean tropical convergence under greenhouse warming, Scientific reports, 4, 6087, doi:10.1038/srep06087, 2014.

Yang, K., Cai, W., Huang, G., Wang, G., Ng, B., and Li, S.: Oceanic Processes in Ocean Temperature Products Key to a Realistic Presentation of Positive Indian Ocean Dipole Nonlinearity, Geophys. Res. Lett., 47, doi:10.1029/2020GL089396, 2020.

Zinke, J., Dullo, W.-C., Heiss, G. A., and Eisenhauer, A.: ENSO and Indian Ocean subtropical dipole variability is recorded in a coral record off southwest Madagascar for the period 1659 to 1995, Earth and Planetary Science Letters, 228, 177–194, doi:10.1016/j.epsl.2004.09.028, 2004.

Zinke, J., Reuning, L., Pfeiffer, M., Wassenburg, J. A., Hardman, E., Jhangeer-Khan, R., Davies, G. R., Ng, C. K. C., and Kroon, D.: A sea surface temperature reconstruction for the southern Indian Ocean trade wind belt from corals in Rodrigues Island (19° S, 63° E), Biogeosciences, 13, 5827–5847, doi:10.5194/bg-13-5827-2016, 2016.